Eur. Phys. J. C (2024) 84:842
https://doi.org/10.1140/epjc/s10052-024-13116-7

THE EUROPEAN PHYSICAL JOURNAL C

Regular Article

Measurement of multijet azimuthal correlations and determination of the strong coupling in proton-proton collisions at $\sqrt{s} = 13\,\text{TeV}$

CMS Collaboration*

CERN, 1211 Geneva 23, Switzerland

Received: 24 April 2024 / Accepted: 11 July 2024 / Published online: 21 August 2024

Abstract A measurement is presented of a ratio observable that provides a measure of the azimuthal correlations among jets with large transverse momentum p_T. This observable is measured in multijet events over the range of $p_\text{T} =$ 360–3170 GeV based on data collected by the CMS experiment in proton-proton collisions at a centre-of-mass energy of 13 TeV, corresponding to an integrated luminosity of 134 fb^{-1}. The results are compared with predictions from Monte Carlo parton-shower event generator simulations, as well as with fixed-order perturbative quantum chromodynamics (pQCD) predictions at next-to-leading-order (NLO) accuracy obtained with different parton distribution functions (PDFs) and corrected for nonperturbative and electroweak effects. Data and theory agree within uncertainties. From the comparison of the measured observable with the pQCD prediction obtained with the NNPDF3.1 NLO PDFs, the strong coupling at the Z boson mass scale is $\alpha_\text{S}(m_\text{Z}) = 0.1177 \pm 0.0013\,(\text{exp})^{+0.0116}_{-0.0073}\,(\text{theo}) = 0.1177^{+0.0117}_{-0.0074}$, where the total uncertainty is dominated by the scale dependence of the fixed-order predictions. A test of the running of α_S in the TeV region shows no deviation from the expected NLO pQCD behaviour.

1 Introduction

In the standard model of particle physics, the strong interaction between partons (quarks and gluons) is described by the theory of quantum chromodynamics (QCD). A key property of the strong interaction is "asymptotic freedom", which characterizes the decreasing value of the coupling $\alpha_\text{S}(Q)$ for increasingly larger momentum transfer Q that corresponds to smaller distances between the interacting partons. This property is a consequence of the non-Abelian nature of QCD, and can be theoretically derived from the renormalization group equations (RGE) [1–3]. Although the RGE cannot predict the absolute value of $\alpha_\text{S}(Q)$, they can accurately determine its evolution as a function of the energy scale Q [4]. By comparing experimental measurements to perturbative QCD (pQCD) predictions for a given observable, the value of $\alpha_\text{S}(Q)$ can be extracted at various scales [5,6]. To compare various $\alpha_\text{S}(Q)$ determinations, it is standard practice to evolve them to a common scale given by the mass of the Z boson, $Q = m_\text{Z}$. The current world-average value of the QCD coupling at this reference scale is $\alpha_\text{S}(m_\text{Z}) = 0.1180 \pm 0.0009$ [5].

This paper reports a new extraction of the $\alpha_\text{S}(Q)$ coupling from multijet measurements at various energy scales in proton-proton (pp) collisions at the CERN LHC. For this purpose, a ratio observable $R_{\Delta\phi}(p_\text{T})$, related to the azimuthal correlations among jets, is measured as a function of the jet transverse momentum p_T. Similar ratio observables, based on either the distance in the plane of rapidity and azimuthal angle among jets, $R_{\Delta R}(p_\text{T})$ [7], or on the dijet azimuthal decorrelations, $R_{\Delta\phi}(H_\text{T})$ [8,9], have already been used to extract the $\alpha_\text{S}(Q)$ coupling at hadron colliders. The $R_{\Delta\phi}(p_\text{T})$ observable is defined as:

$$R_{\Delta\phi}(p_\text{T}) = \frac{\sum_{i=1}^{N_\text{jet}(p_\text{T})} N^{(i)}_\text{nbr}(\Delta\phi,\, p^\text{nbr}_\text{Tmin})}{N_\text{jet}(p_\text{T})}, \tag{1}$$

where the denominator $N_\text{jet}(p_\text{T})$ simply counts the number of jets in a given jet p_T bin, and the numerator sums the number of neighbouring jets, $N^{(i)}_\text{nbr}$, around each jet i in the same p_T bin. A neighbouring jet must exceed a minimum transverse momentum of p^nbr_Tmin and be separated from jet i within a specified interval of azimuthal distance $\Delta\phi$: $\Delta\phi_\text{min} < \Delta\phi < \Delta\phi_\text{max}$. In fixed-order predictions of jet production based on pQCD calculations, the leading-order (LO) $2 \to 2$ process is characterized by an azimuthal separation of $\Delta\phi = \pi$. Since the sum in the numerator runs over all jets, this would lead to two entries at $p_\text{T} = p_{\text{T},1} = p_{\text{T},2}$. At next-to-leading order (NLO), the radiation of a third hard parton can give rise to a 3-jet topology with $\Delta\phi$ between $2\pi/3$ and π with respect

* e-mail: cms-publication-committee-chair@cern.ch (corresponding author)

to the jet opposite to the hemisphere with radiation (Fig. 1, right diagrams). Hence, by fixing the azimuthal distance for neighbouring jets to $2\pi/3 < \Delta\phi < 7\pi/8$ in Eq. (1), the dijet case is avoided, and the numerator is different from zero only for events with three jets or more, whose LO cross section is proportional to α_S^3. Also here, a jet pair fulfilling both the selection in $p_{\mathrm{Tmin}}^{\mathrm{nbr}}$ and in $\Delta\phi$ leads to two entries, but potentially at different jet p_T values. On the other hand, the denominator corresponds to the inclusive jet cross section, which at LO is proportional to α_S^2, such that the $R_{\Delta\phi}(p_T)$ observable is directly proportional to α_S, at the lowest order. A representative illustration, indicating the entries to the numerator and denominator of the $R_{\Delta\phi}(p_T)$ ratio, is shown in the left and right panels of Fig. 1 for a 2-jet and a 3-jet event, respectively.

In the ratio defined by Eq. (1) many experimental systematic uncertainties – such as those from the integrated luminosity, the jet energy scale (JES), and the jet energy resolution (JER) – cancel entirely or to a large extent. In addition, theoretical uncertainties – such as nonperturbative (NP) and parton distribution function (PDF) uncertainties – are reduced.

To rigorously account for correlations between the numerator and denominator, it is useful to consider the more general, two-dimensional jet-counting quantity, $N(p_T, n)$, which is a function of the i-th jet's p_T and of the number n of neighbouring jets that satisfy the additional selection criteria for $p_{\mathrm{Tmin}}^{\mathrm{nbr}}$ and $\Delta\phi$. Then, using $N(p_T, n)$, it can be shown that the $R_{\Delta\phi}(p_T)$ observable can be also formulated as:

$$R_{\Delta\phi}(p_T) = \frac{\sum_n n N(p_T, n)}{\sum_n N(p_T, n)}. \tag{2}$$

Such a definition allows a multidimensional unfolding of the more general quantity $N(p_T, n)$ to be performed, instead of a separate unfolding of the numerator and denominator of Eq. (1).

The measurement is performed using data collected with the CMS detector, during the LHC Run 2 data-taking period (2016–2018), corresponding to an integrated luminosity of 134 fb^{-1} at a centre-of-mass energy of 13 TeV [10–12]. Previous determinations of the strong coupling constant $\alpha_S(m_Z)$ using jets at hadron colliders have been reported by the CDF [13] and D0 [7,14] Collaborations in proton-antiproton collisions at $\sqrt{s} = 1.8$ and 1.96 TeV at the Fermilab Tevatron. At the LHC, determinations have been reported using pp collision data from the ATLAS and CMS Collaborations at $\sqrt{s} = 7$ [15–22], 8 [9,21–25], and 13 [26–29,29–32] TeV.

The paper is organized as follows. In Sect. 2 a brief description of the CMS detector is given. In Sect. 3 the event reconstruction is described. Section 4 details the measurement of the $R_{\Delta\phi}(p_T)$ observable. Experimental results and theoretical predictions for the $R_{\Delta\phi}(p_T)$ observable are compared in Sect. 5. The determination of $\alpha_S(m_Z)$ and the investigation of the running of the $\alpha_S(Q)$ coupling are presented in Sect. 6. Finally, a summary of the paper is given in Sect. 7.

Tabulated results are provided in the HEPData record for this analysis [33].

2 The CMS detector

The central feature of the CMS apparatus is a superconducting solenoid of 6 m internal diameter, providing a magnetic field of 3.8 T. Within the solenoid volume are a silicon pixel and strip tracker, a lead tungstate crystal electromagnetic calorimeter (ECAL), and a brass and scintillator hadron calorimeter (HCAL), each composed of a barrel and two endcap sections. Forward calorimeters extend the pseudorapidity coverage provided by the barrel and endcap detectors. Muons are measured in gas-ionization detectors embedded in the steel flux-return yoke outside the solenoid.

The electromagnetic calorimeter consists of 75 848 lead tungstate crystals, which provide coverage in pseudorapidity $|\eta| < 1.48$ in a barrel region (EB) and $1.48 < |\eta| < 3.0$ in two endcap regions (EE). Preshower detectors consisting of two planes of silicon sensors interleaved with a total of three radiation lengths of lead are located in front of each EE detector.

In the region $|\eta| < 1.74$, the HCAL cells have widths of 0.087 in pseudorapidity and 0.087 in azimuth (ϕ). In the η–ϕ plane, and for $|\eta| < 1.48$, the HCAL cells map on to 5×5 arrays of ECAL crystals to form calorimeter towers projecting radially outwards from close to the nominal interaction point. For $|\eta| > 1.74$, the coverage of the towers increases progressively to a maximum of 0.174 in $\Delta\eta$ and $\Delta\phi$. A more detailed description of the CMS detector, together with a definition of the coordinate system used and the relevant kinematic variables, can be found in Ref. [34].

Events of interest are selected using a two-tiered trigger system. The first level (L1), composed of custom hardware processors, uses information from the calorimeters and muon detectors to select events at a rate of around 100 kHz within a fixed latency of about 4 μs [35]. The second level, known as the high-level trigger (HLT), consists of a farm of processors running a version of the full event reconstruction software optimized for fast processing and reduces the event rate to around 1 kHz before data storage [36].

3 Event reconstruction

The global event reconstruction – also called particle-flow (PF) event reconstruction [37] – aims to reconstruct and identify each individual particle in an event, with an optimized combination of all subdetector information. In this process, the identification of the particle type (photon, elec-

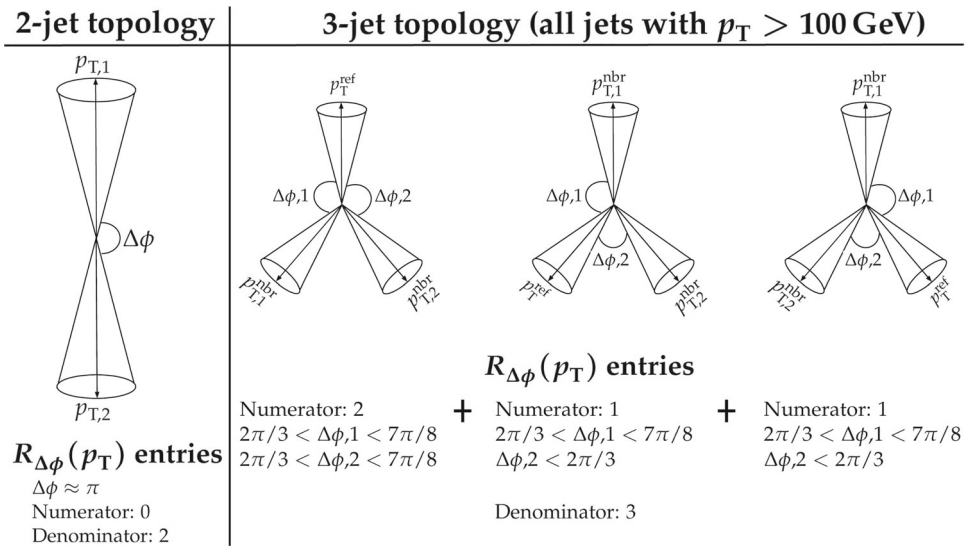

Fig. 1 Example of the number of entries contributing to the numerator and denominator of the $R_{\Delta\phi}(p_T)$ ratio, Eq. (1), for 2-jet (left) and 3-jet (right) events, with all jets having $p_T > p_{Tmin}^{nbr} = 100$ GeV. The 2-jet topology does not contribute (null numerator) to the $R_{\Delta\phi}(p_T)$ ratio when the azimuthal distance for neighbouring jets is fixed to $2\pi/3 < \Delta\phi < 7\pi/8$. In the 3-jet topology, each jet is considered as a reference, and its azimuthal separations ($\Delta\phi,1$ and $\Delta\phi,2$) to other neighbouring jets (with $p_{T,1}^{nbr}$ and $p_{T,2}^{nbr}$) are computed. Each neighbouring jet with $\Delta\phi$ within the specified interval increments the entries of the numerator, whereas the denominator simply counts the number of jets in the event

tron, muon, charged hadron, neutral hadron) plays an important role in the determination of the particle direction and energy. Photons (e.g., coming from π^0decays or from electron bremsstrahlung) are identified as ECAL energy clusters not linked to the extrapolation of any charged particle trajectory to the ECAL. Electrons (e.g., coming from photon conversions in the tracker material or from bottom quark (b) hadron semileptonic decays) are identified as a primary charged particle track and potentially many ECAL energy clusters corresponding to this track extrapolation to the ECAL and to possible bremsstrahlung photons emitted along the way through the tracker material. Muons (e.g., from b hadron semileptonic decays) are identified as tracks in the central tracker consistent with either a track or several hits in the muon system, and associated with calorimeter deposits compatible with the muon hypothesis. Charged hadrons are identified as charged particle tracks neither identified as electrons, nor as muons. Finally, neutral hadrons are identified as HCAL energy clusters not linked to any charged-hadron trajectory, or as a combined ECAL and HCAL energy excess with respect to the expected charged-hadron energy deposit.

The energy of photons is obtained from the ECAL measurement. The energy of electrons is determined from a combination of the track momentum at the main interaction vertex, the corresponding ECAL cluster energy, and the energy sum of all bremsstrahlung photons attached to the track. The energy of muons is obtained from the corresponding track momentum. The energy of charged hadrons is determined from a combination of the track momentum and the corresponding ECAL and HCAL energies, corrected for the response function of the calorimeters to hadronic showers. Finally, the energy of neutral hadrons is obtained from the corresponding corrected ECAL and HCAL energies.

The primary vertex (PV) is taken to be the vertex corresponding to the hardest scattering in the event, evaluated using tracking information alone, as described in Section 9.4.1 of Ref. [38]. For each event, hadronic jets are clustered from the reconstructed particle candidates using the infrared and collinear safe anti-k_T algorithm [39,40] with a distance parameter of $R = 0.7$. This choice of the parameter R enables the compatibility with previous results from the CMS Collaboration at $\sqrt{s} = 7$ [16] and 13 [30] TeV. Jet momentum is determined as the vectorial sum of all particle momenta in the jet, and is found from simulation to be, on average, within 5 to 10% of the true momentum over the whole p_T spectrum and detector acceptance. Additional pp interactions within the same, or nearby, bunch crossings (pileup) can contribute additional tracks and calorimetric energy depositions to the jet momentum. To mitigate this effect, charged particles identified to be originating from pileup vertices are discarded, and an offset correction is applied to correct for the remaining contributions [41]. The JES corrections are derived from simulation to bring the measured response of jets to that of particle-level jets on average. In situ measurements of the momentum balance in dijet, photon + jet, Z + jet, and multijet events are used to account for any residual differences in the jet energy scale between the measured data and simulation [42]. The jet energy resolution amounts typically to

Table 1 The different HLT p_T thresholds used in the measurement and the corresponding integrated luminosities for each data-taking year

p_T^{thresh} (GeV)		40	60	80	140	200	260	320	400	450	500
$\mathcal{L}$ (pb^{-1})	2016	0.0497	0.328	1.00	10.1	85.8	518	1526	4590	33,500	–
	2017	0.182	0.505	2.53	26.6	189	469	1230	7690	9660	41,500
	2018	0.0151	0.419	2.17	47.1	202	466	1240	3720	7390	59,800

15–20% at 30 GeV, 10% at 100 GeV, and 5% at 1 TeV [42]. Additional selection criteria are applied to each jet to remove jets potentially dominated by anomalous contributions from various subdetector components or reconstruction failures [43].

The missing transverse momentum vector $\vec{p}_T^{miss}$ is computed as the negative vector sum of the transverse momenta of all the PF candidates in an event, and its magnitude is denoted as p_T^{miss} [44]. The $\vec{p}_T^{miss}$ is modified to account for corrections to the energy scale of the reconstructed jets in the event.

During the 2016-2017 data taking, a gradual shift in the timing of the inputs of the ECAL L1 trigger in the region at $|\eta| > 2.0$ caused a specific trigger inefficiency [45], called "prefiring" hereafter. For events containing a jet with $p_T \gtrsim 100$ GeV in the region $2.5 < |\eta| < 3.0$, the efficiency loss is ≈10–20%, depending on p_T, η, and data-taking period.

4 Data analysis

4.1 Event selection criteria

Each event is required to have at least one offline-reconstructed PV with z coordinate satisfying the criterion $|z_{PV}| < 24$ cm and radial distance from the interaction point $\rho_{PV} < 2$ cm. Anomalous high-p_T^{miss} events can be due to a variety of reconstruction failures, detector malfunctions, or noncollision backgrounds. Such events are rejected by event filters that are designed to identify more than 85–90% of the spurious high-p_T^{miss} events with a mistagging rate less than 0.1% [44]. Only events that have been accepted by at least one single-jet trigger path (described in Sect. 4.2) are included in the measurement. For the rejection of poorly reconstructed jets and jets originating from detector noise, additional quality criteria are applied to them based on their constituents [43].

The measurement is based on an inclusive jet sample that contains only jets reconstructed within the rapidity range $|y| < 2.5$ and with transverse momenta $p_T > 50$ GeV. The p_{Tmin}^{nbr} threshold and azimuthal separation interval for neighbouring jets as defined in Eq. (1), are set to 100 GeV and $2\pi/3 < \Delta\phi < 7\pi/8$, respectively. This choice was motivated by statistical optimization, extending the phase space as much as possible, and guaranteeing that the NLO predictions remain valid and soft effects are negligible.

4.2 Triggers

The analysis is based on single-jet triggers that require at least one jet with p_T above a given threshold (p_T^{thresh}) to be present in the event. Table 1 shows the different HLT thresholds along with the effective integrated luminosities recorded by the triggers for 2016, 2017 and 2018. All triggers in Table 1 were prescaled, apart from trigger 450 for 2016, and trigger 500 for 2017 and 2018. The efficiency for each trigger is estimated as a function of leading-jet p_T using a lower-threshold trigger, except for the lowest-threshold trigger efficiency. The latter is estimated using a tag-and-probe method applied to dijet topologies, which counts the jets reconstructed with the offline PF algorithm that can be matched to HLT jets, considering only the jets leading and subleading in p_T. The data consist of events selected with a combination of triggers in mutually exclusive leading-jet p_T intervals. The usage of a specific trigger is enabled only in phase-space regions where its efficiency is larger than 99.5% and disabled in phase-space regions where the efficiency of a higher-threshold trigger is larger than 99.5%. The jet-counting variables are combined event-by-event by applying weights to account for the trigger prescales of each data sample.

4.3 Unfolding

To compare the experimental data with theoretical predictions, the measured distributions must be corrected for detector effects, such as finite p_T resolution and limited detector acceptance. The detector effects are parameterized through a response matrix built from simulated event samples using PYTHIA 8.240 [46] with tunes CUETP8M1 [47] and CP5 [48], where reconstructed-level jets are matched to generator-level jets as explained next. First, the generated jets in each event are ordered by decreasing p_T. Then, each generated jet is matched to the reconstructed jet with the highest p_T, within a cone of radius $\Delta R = \sqrt{(\Delta\eta)^2 + (\Delta\phi)^2} = 0.35$ (where $\Delta\eta$ and $\Delta\phi$ are the angular differences in pseudorapidity and azimuthal angle between the generated and reconstructed jets). The probability matrix $\boldsymbol{A}$ corresponds to the row-by-row normalized response matrix. Each ele-

Table 2 Values of the $R_{\Delta\phi}(p_{\mathrm{T}})$ observable in different p_{T} intervals, and associated experimental uncertainties

p_{T} (GeV)	$R_{\Delta\phi}(p_{\mathrm{T}})$	Stat. (%)	JES (%)	Prefiring (%)	JER (%)	PU (%)	$\mathrm{MC}_{\mathrm{model}}$ (%)
360–430	0.25	0.26	0.74	0.06	0.08	0.01	–
430–510	0.26	0.23	0.69	0.09	0.06	0.02	–
510–600	0.27	0.19	0.67	0.12	0.05	0.02	–
600–700	0.27	0.18	0.66	0.13	0.04	0.02	0.01
700–800	0.28	0.18	0.65	0.12	0.04	0.02	0.01
800–920	0.28	0.20	0.65	0.10	0.04	0.02	0.01
920–1050	0.27	0.27	0.66	0.07	0.05	0.02	–
1050–1190	0.27	0.39	0.67	0.05	0.06	0.02	–
1190–1340	0.27	0.58	0.70	0.03	0.07	0.02	–
1340–1500	0.26	0.90	0.75	0.02	0.08	0.02	–
1500–1680	0.26	1.34	0.84	0.01	0.11	0.02	–
1680–1870	0.25	2.16	0.98	–	0.14	0.02	–
1870–2070	0.24	3.42	1.21	–	0.19	0.02	–
2070–2300	0.21	5.66	1.62	–	0.27	0.02	–
2300–2560	0.22	8.23	2.36	–	0.39	0.02	–
2560–3170	0.21	10.49	5.00	–	0.77	0.01	–

ment A_{ij} represents the probability of a jet produced in (generator-level) bin j to be observed in (reconstructed-level) bin i. The detector effects are corrected through an unfolding procedure that accounts for bin migrations, background (fake jets, i.e., reconstructed-level jets that could not be matched to generator-level jets), and inefficiencies (missed jets, i.e., generator-level jets that could not be matched to reconstructed-level jets), and corrects the measurement from the detector level to the level of stable particles (except neutrinos) with mean decay-lengths larger than $c\tau = 10\,\mathrm{mm}$ (where τ denotes the mean proper lifetime of the particle).

The unfolding procedure is implemented using the TUNFOLD package [49]. The determination of the particle-level distribution ($\boldsymbol{x}$) is performed with the matrix pseudoinverse method [50] using a detector-level distribution ($\boldsymbol{y}$) with twice the number of bins of the particle-level distribution. The latter are defined in Table 2 (first column) and are chosen to ensure that the bin sizes remain at least twice as large as the jet p_{T} resolution. The unfolding solution arises from the minimization of the quantity

$$\chi^2 = (\boldsymbol{Ax} + \boldsymbol{b} - \boldsymbol{y})^{\boldsymbol{T}} \, (\boldsymbol{V^{-1}}) \, (\boldsymbol{Ax} + \boldsymbol{b} - \boldsymbol{y}), \tag{3}$$

where $\boldsymbol{b}$ is the background obtained from simulated events, and $\boldsymbol{V}$ is the covariance matrix (corrected for the background) of the detector-level data including their statistical uncertainties and correlations. Instead of unfolding separately the numerator and denominator of Eq. (1), a multidimensional unfolding of the more general, equivalent quantity $N(p_{\mathrm{T}}, n)$ is performed, which rigorously accounts for the numerator-denominator statistical correlations following Eq. (2).

Figure 2 shows the probability matrix for the $N(p_{\mathrm{T}}, n)$ quantity. The number of events with $n \geq 4$ is small, and $n = 3$ is the maximum number of neighbouring jets shown here. The condition number (defined as the absolute value of the ratio between the largest and smallest matrix eigenvalues) for the matrix $\boldsymbol{A}$ is ≈5.5, which means that the unfolding problem is well-conditioned, and therefore no additional regularization is required.

4.4 Experimental uncertainties

The experimental uncertainties contain statistical and systematic sources that propagate to the measured distributions. The statistical uncertainties are obtained from the covariance matrix, extracted at the particle level from the $N(p_{\mathrm{T}}, n)$ distribution along with the $R_{\Delta\phi}(p_{\mathrm{T}})$ observable, as described in Sect. 4.3. The bin-to-bin correlation matrix at the particle level is shown in Fig. 3, where the value 1 (−1) corresponds to fully (anti)correlated bins. The diagonal elements of the correlation matrix are by construction always unity, and the off-diagonal elements represent the bin-to-bin (anti)correlations, where the highest (lowest) value is 0.49 (−0.57). The statistical uncertainties in the $R_{\Delta\phi}(p_{\mathrm{T}})$ measurement remain below 1% up to ≈1.5 TeV increasing to about 10% at ≈3 TeV.

The calibration of the reconstructed jet energy is performed through a series of successive stages implemented in the JES correction procedure [42], as described in Sect. 3. The JES uncertainty is composed of 27 individual uncorrelated contributions, which are investigated one-by-one considering a ±1 standard-deviation variation from their nominal value. Each variation is applied at the detector level and propagated

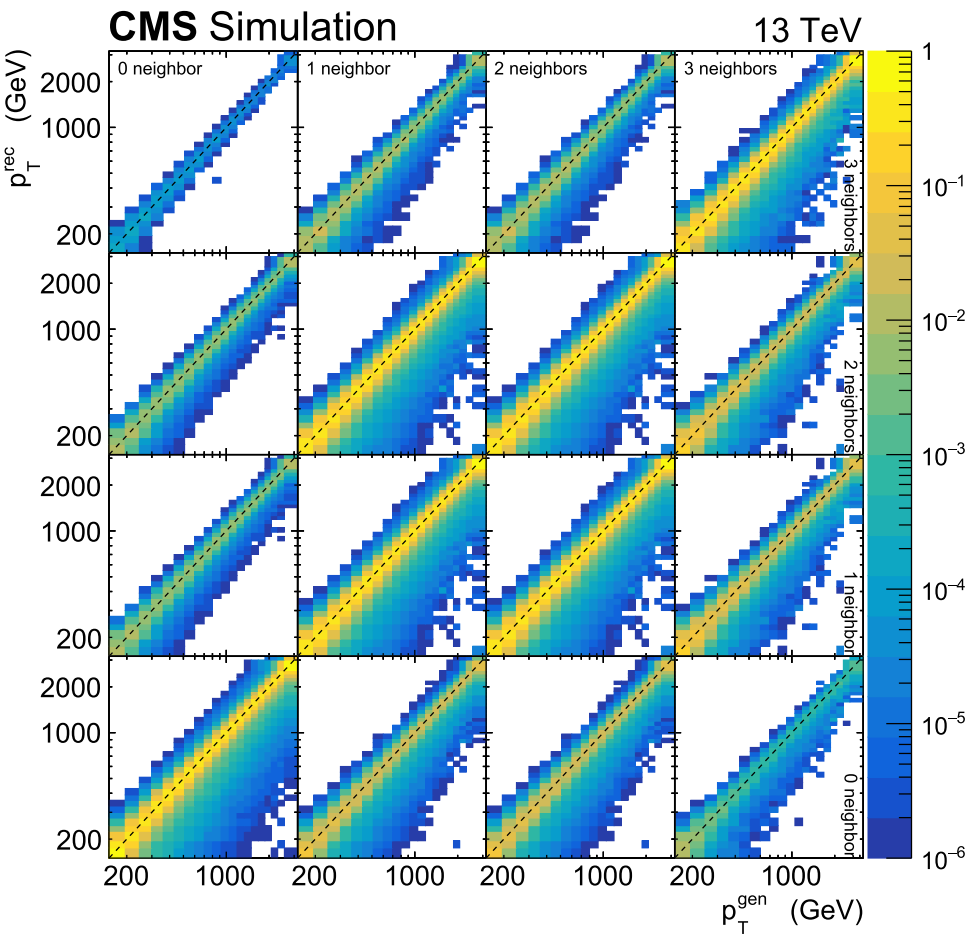

Fig. 2 Probability matrix for the $N(p_T, n)$ distribution built using PYTHIA8 simulated events. The horizontal axis corresponds to the generator-level jet p_T, and the vertical axis to the reconstructed-level jet p_T. The 4×4 structure of the matrix corresponds to the bins of neighbouring jets n (labelled in the uppermost row and rightmost column), and indicates migrations among those bins. The horizontal and vertical axes of each cell correspond to the p_T of the jets, and each cell indicates the migrations among the jet p_T bins. The range of colours covers from 10^{-6} to 1, and indicates the probability of migrations from a given (generator) particle-level bin to the corresponding (reconstructed) detector-level bin

to the particle-level measurement by repeating the unfolding procedure. Finally, the total JES uncertainty is computed as the quadratic sum of individual JES uncertainty sources, and remains below 1% up to ≈1.5 TeV increasing to about 5% at ≈3 TeV. Additional variations of the trigger prefiring corrections described in Sect. 3 are applied in the same manner. The uncertainties from prefiring corrections in the $R_{\Delta\phi}(p_T)$ measurement are smaller than 0.13%.

In simulated samples, a detailed modelling of the CMS detector is included based on the GEANT4 toolkit [51]. The JER obtained in the detector simulation is generally better than that in the actual detector. Therefore, the energy of reconstructed jets in simulation is smeared out, so that the simulated JER matches the one measured in experimental data. The JER uncertainty is estimated by varying the smearing factors within ±1 standard deviations from their nominal values, and propagated to the particle-level measurement by repeating the unfolding procedure. The JER uncertainty in the $R_{\Delta\phi}(p_T)$ measurement is below 0.8%.

The probability distribution for the number of pp interactions per bunch crossing is represented by pileup (PU) profiles. To account for differences between the measured and simulated PU profiles, the simulated events are reweighted using the PU distribution of the experimental data as a reference. An additional systematic uncertainty, which remains below 0.03%, is evaluated by varying the PU profile correction in the simulation. The model dependence introduced by unfolding is estimated from the difference in the $R_{\Delta\phi}(p_T)$ distribution unfolded with response matrices obtained from PYTHIA8 and MADGRAPH5_aMC@NLO 2.6 [52,53] interfaced with PYTHIA8. Additionally, the model dependence for inefficiencies (missed jets) and backgrounds (misreconstructed jets) is studied by varying separately their rates within an estimate of 5%, which largely covers the model dependence of migrations in and out of the phase space. The total model dependence uncertainties (MC_{model}) are negligible (<0.01%) compared with other uncertainties for the bulk of the spectrum. The trigger efficiency uncertainties are also negligible in the $R_{\Delta\phi}(p_T)$ measurement. The $R_{\Delta\phi}(p_T)$ observable values along with all the experimental uncertainties are shown in Table 2.

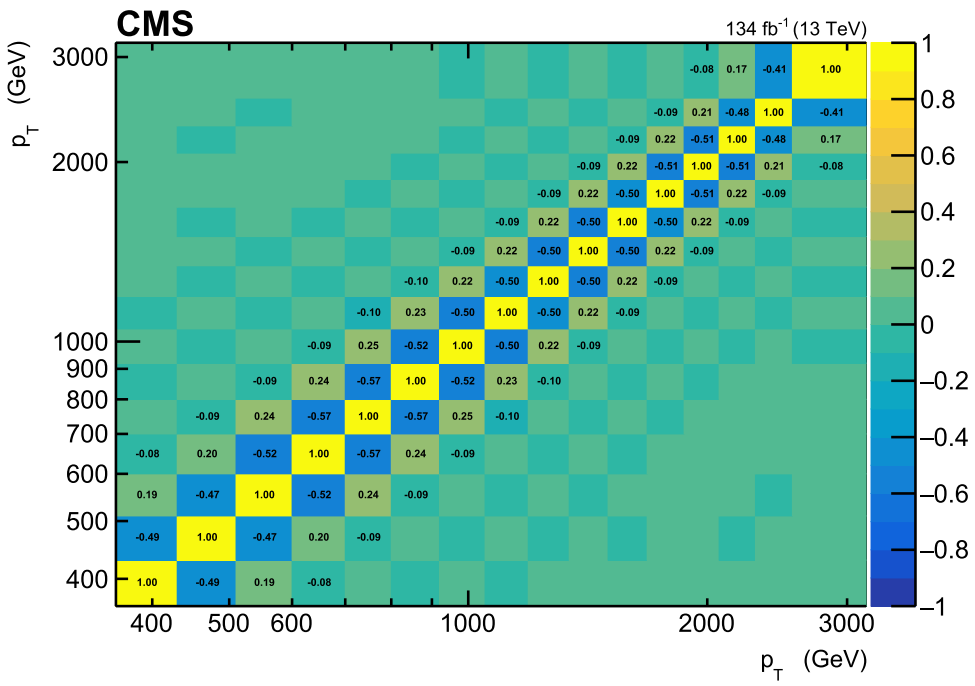

Fig. 3 Bin-to-bin correlation matrix for the $R_{\Delta\phi}(p_{\mathrm{T}})$ distribution at the particle level, where the value 1 (−1) corresponds to fully (anti)correlated bins. For illustration purposes, only bins with (anti)correlations larger (smaller) than 0.05 (−0.05) are shown also as text

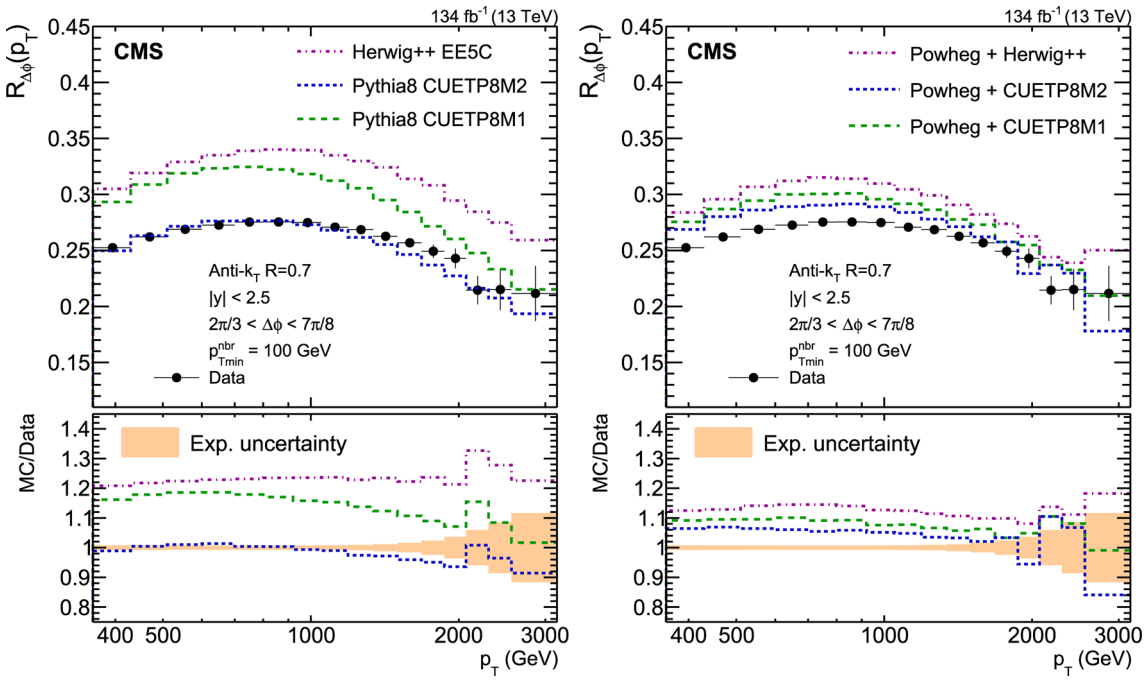

Fig. 4 The $R_{\Delta\phi}(p_{\mathrm{T}})$ observable as a function of p_{T}, compared with MC generator predictions at LO (left) and at NLO (right) accuracy. The LO predictions are obtained with PYTHIA8 tunes CUETP8M1 and CUETP8M2, and HERWIG++ tune UE-EE-5-CTEQ6L1 MC event generators. The NLO predictions are obtained with POWHEG interfaced with each of the aforementioned MC event generators. The experimental data are represented with black dots and the MC predictions with coloured lines. The lower panel of each plot shows the ratio between MC predictions and experimental data. The total experimental uncertainties are indicated by the vertical error bars (upper panels) and coloured band (lower panels) correspondingly

Table 3 Default and range of $\alpha_S(m_Z)$ values used in the different NLO PDF sets

PDF set	Default $\alpha_S(m_Z)$	Alternative $\alpha_S(m_Z)$
ABMP16 [78]	0.1191	0.114–0.123
CT18 [79]	0.1180	0.110–0.124
MSHT20 [80]	0.1200	0.108–0.130
NNPDF3.1 [81]	0.1180	0.106–0.130

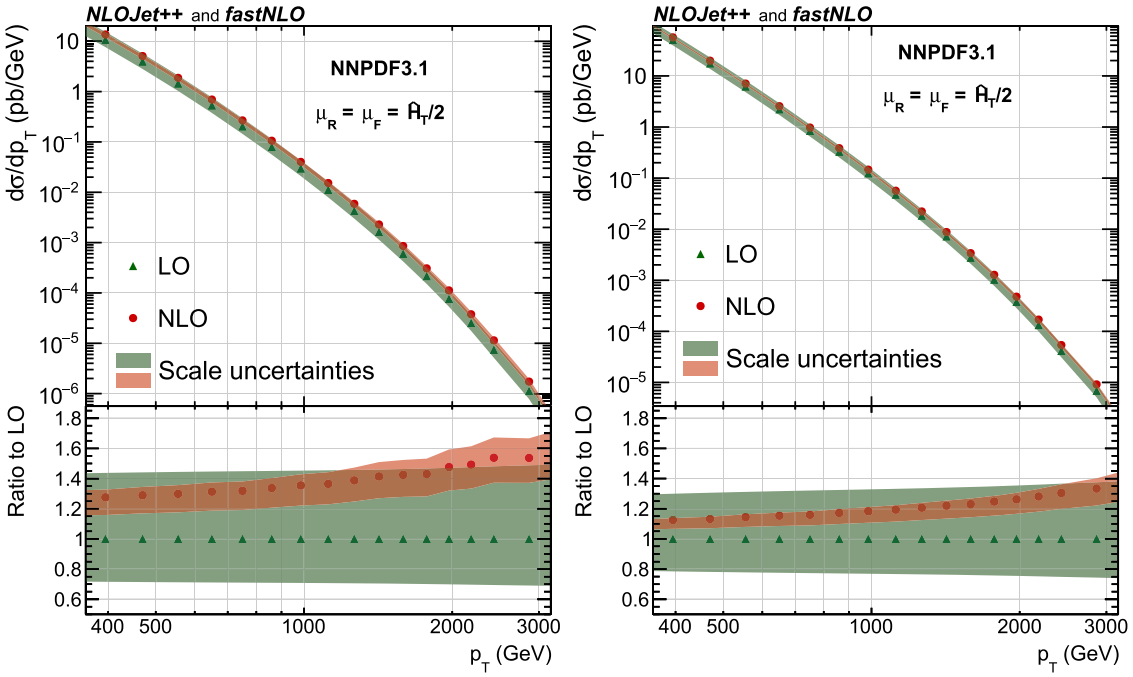

Fig. 5 Theoretical predictions for the cross sections corresponding to the numerator (left) and denominator (right) of the $R_{\Delta\phi}(p_T)$ ratio, Eq. (1), obtained using the NNPDF3.1 NLO PDF set. The coloured bands represent the LO and NLO scale uncertainties derived with a six-point variation of μ_R and μ_F from the central reference value. The lower panels show the ratios to the respective LO predictions

5 Theoretical predictions

5.1 Monte Carlo event generators predictions

Experimental data are compared with predictions from HERWIG++ 2.7.1 [54], PYTHIA 8.240 [46], and POWHEG 2.0 [55] Monte Carlo (MC) event generators obtained using the RIVET toolkit [56]. The HERWIG++ event generator computes the matrix elements (MEs) at LO accuracy for $2 \to 2$ QCD scattering processes. The parton shower (PS) is simulated through successive angular-ordered emissions, and the cluster fragmentation model [57] is used for the hadronization. The underlying event (UE) activity is obtained from the simulation of multiparton interactions (MPIs) tuned to experimental data. The set of HERWIG++ parameters used in this analysis is that of the UE-EE-5-CTEQ6L1 tune [58] based on the CTEQ6.1M LO PDF set [59]. Similarly to HERWIG++, in PYTHIA8 the MEs are calculated at LO accuracy for $2 \to 2$ QCD scattering processes. The PS is simulated through successive p_T-ordered emissions and the hadronization mechanism employs the Lund string model [60]. Two different sets of parameters are used for PYTHIA8, the CUETP8M1 tune [47] based on the NNPDF2.3 LO PDF set [61,62] and the CUETP8M2 tune [63] based on the NNPDF3.0 LO PDF set [64]. The POWHEG [65,66] generator, based on the POWHEG BOX [55], generates $2 \to 2$ matrix elements at NLO accuracy, as well as $2 \to 3$ matrix elements at LO accuracy and uses the NNPDF3.0 NLO PDF set [64]. To simulate the PS, hadronization, and MPI processes, POWHEG is interfaced either with PYTHIA8 or with HERWIG++.

Figure 4 (left) shows the particle-level data for the $R_{\Delta\phi}(p_T)$ observable compared with the predictions of PYTHIA8 tunes CUETP8M1 and CUETP8M2, and HERWIG++ tune UE-EE-5-CTEQ6L1 LO MC event generators. The lower panels show the corresponding ratios between the MC predictions and the measured data. Figure 4 (right) illustrates the particle-level $R_{\Delta\phi}(p_T)$ observable compared with POWHEG interfaced with PYTHIA8 tunes CUETP8M1 and CUETP8M2,

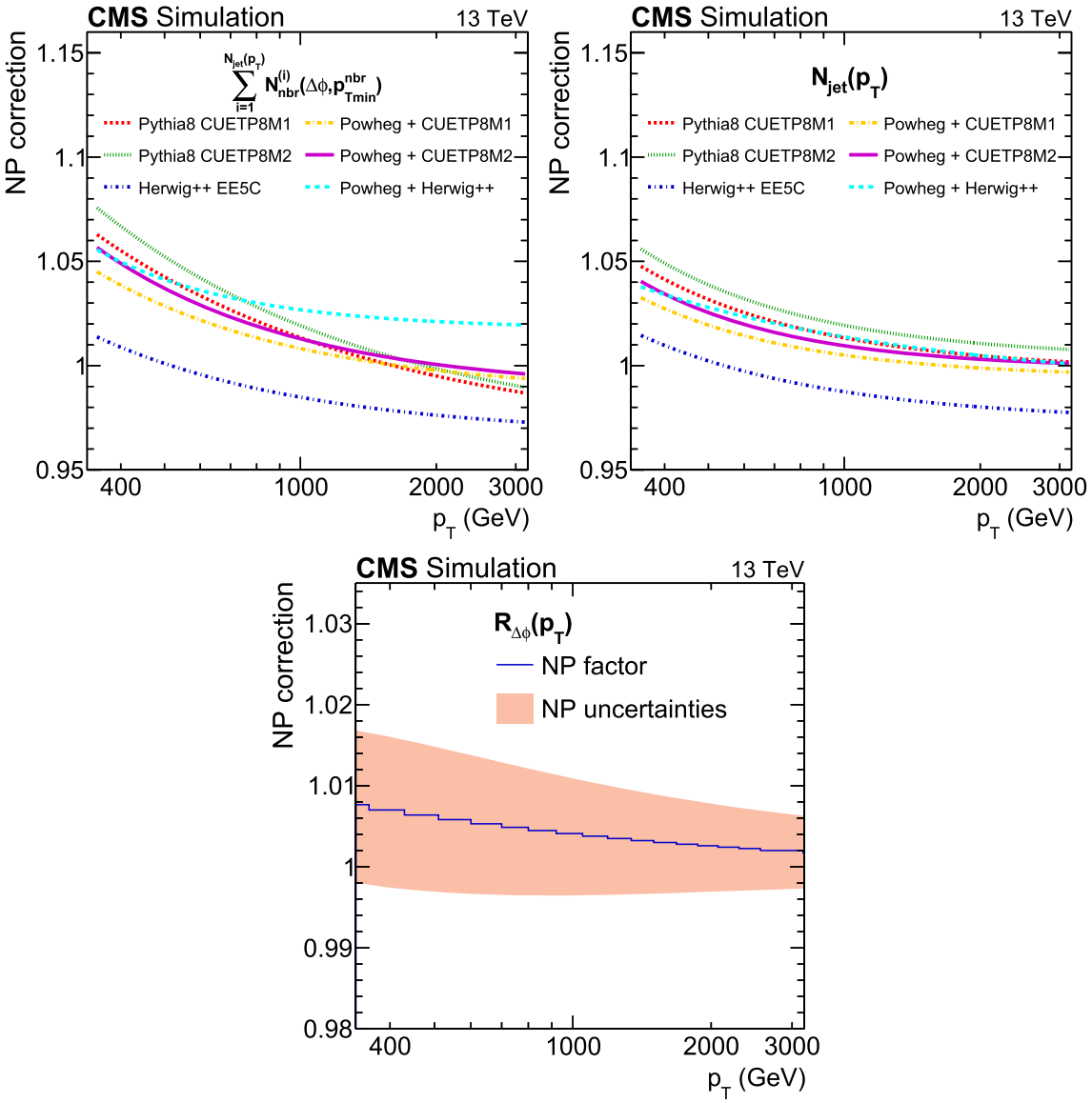

Fig. 6 Nonperturbative correction factors for the numerator (upper left) and denominator (upper right) of the $R_{\Delta\phi}(p_T)$ ratio, Eq. (1), using PYTHIA8 with tunes CUETP8M1 and CUETP8M2, HERWIG++ with tune UE-EE-5-CTEQ6L1, and POWHEG interfaced with each of them. The lower plot shows the NP correction factors (blue line) for $R_{\Delta\phi}(p_T)$ and their uncertainties

and HERWIG++ tune UE-EE-5-CTEQ6L1 results. The corresponding lower panels show the ratios between the POWHEG predictions and the measurement. The coloured band on both lower panels represents the total experimental uncertainties.

From 360 up to around 800 GeV, the $R_{\Delta\phi}(p_T)$ distribution rises as the phase space for the production of a third jet increases. Then, the distribution reaches a plateau up to around 1200 GeV, followed by a decrease due to the running of α_S, and the reduced amount of gluon scatterings.

The predictions from LO HERWIG++ and LO PYTHIA8 tune CUETP8M1 overestimate the measurement by ≈20% and ≈12–18%, respectively. On the other hand, the predictions from the (LO) PYTHIA8 tune CUETP8M2 give a good description of the data. Besides the PDF set, the main differences between the parameters of the two PYTHIA8 tunes are the value of α_S used for the initial-state shower α_S^{ISR}, the MPI infrared regularization scale p_{T0}^{ref}, and the amount of colour reconnection. Among the NLO MC predictions based on POWHEG, the POWHEG interfaced with PYTHIA8 tune CUETP8M2 gives the best description, being ≈5–6% away from the measurement. Finally, POWHEG interfaced with HERWIG++ tune UE-EE-5-CTEQ6L1 or with PYTHIA8 tune CUETP8M1 overestimate the $R_{\Delta\phi}(p_T)$ measurement by ≈12% and ≈10%, respectively.

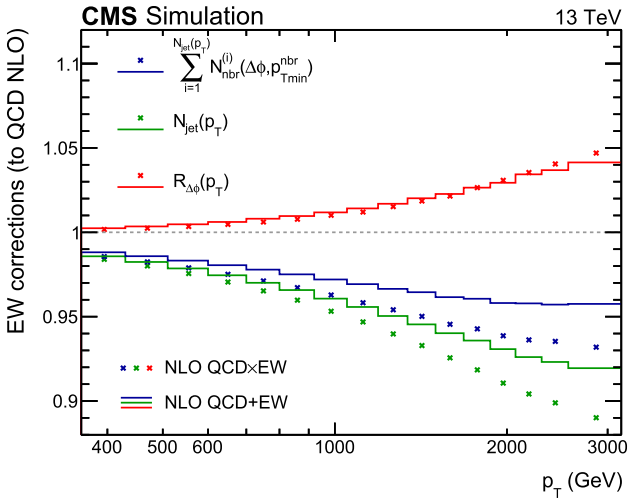

Fig. 7 Electroweak corrections for the numerator (blue) and denominator (green) of Eq. (1), and for the $R_{\Delta\phi}(p_T)$ ratio itself (red). The solid lines correspond to the additive combination of NLO EW corrections to the QCD process (NLO QCD + EW), and the markers represent the multiplicative combination (NLO QCD × EW)

5.2 Fixed-order predictions

Fixed-order theoretical predictions for the $R_{\Delta\phi}(p_T)$ observable are obtained up to NLO accuracy in pQCD with the NLOJET++ program [67,68] within the FASTNLO framework [69,70]. The predictions are extracted for several PDF sets available via the LHAPDF library [71], using their default value for the strong coupling constant $\alpha_S(m_Z)$, and alternative values, as shown in Table 3. The central reference values μ_0 for the renormalization (μ_R) and factorization (μ_F) scales are defined as:

$$\mu_R = \mu_F = \hat{H}_T/2, \tag{4}$$

where $\hat{H}_T$ is the scalar sum of the transverse momenta of all partons in the event. This choice follows recommendations detailed in Ref. [72], which favour $\hat{H}_T$ over $p_{T,jet}$ and discourage the use of $p_{T,max} = p_{T,1}$ as the central scale choice for inclusive jet cross sections. For 3-jet ratio observables such as $R_{\Delta\phi}(p_T)$, Refs. [73,74] conclude that $\hat{H}_T/2$ is slightly preferred for comparisons with theoretical predictions at next-to-NLO accuracy. The uncertainties related to missing higher-order terms of the perturbative series are estimated using the conventional recipe [75–77], i.e., by varying μ_R and μ_F around the reference scale μ_0 within six combinations: $(\mu_R/\mu_0, \mu_F/\mu_0) = (1/2, 1/2), (1/2, 1), (1, 1/2), (1, 2), (2, 1), (2, 2)$. An envelope is constructed from the various combinations, where the edges define the scale uncertainties.

Theoretical calculations are performed separately for the cross sections corresponding to the jet counts in the numerator and denominator of the $R_{\Delta\phi}(p_T)$ ratio defined in Eq. (1). The predictions using NNPDF3.1 for the numerator (left) and denominator (right) differential cross sections ($d\sigma/dp_T$) at LO and NLO accuracy are shown in Fig. 5, along with the scale uncertainties (coloured bands). The lower panels in this figure display the ratios to the respective LO predictions, where the so-called NLO pQCD K factors (NLO/LO) are about 1.30–1.55 for the numerator and 1.20–1.35 for the denominator (1.08–1.15 for their ratio). The LO and NLO scale uncertainty bands overlap over the whole phase space. The NLO scale uncertainties are in the range 9–17% for the numerator and 5–10% for the denominator.

To compare fixed-order predictions at parton level with unfolded data, the former must be corrected for NP effects due to MPI and hadronization (HAD). Based on PS generators, the NP correction factors are evaluated from the ratio of the nominal over the generated cross sections when MPI and HAD effects are switched off:

$$C^{NP} = \frac{\sigma^{PS+MPI+HAD}}{\sigma^{PS}}. \tag{5}$$

The model dependence of C^{NP} is investigated using different MC event generators, namely PYTHIA8 with tunes CUETP8M1 and CUETP8M2, HERWIG++ with tune UE-EE-5-CTEQ6L1, and POWHEG interfaced with each one of them. A simple polynomial function $a + bp_T^c$ (where a, b, and c are free parameters) is used to parameterize the dependence of C^{NP} on jet p_T for each MC event generator, to avoid statistical fluctuations in less populated regions of phase space. An envelope is constructed from the different MC predictions, where the central values are identified as the NP correction factors C^{NP} and the edges define the corresponding uncertainties. Figure 6 shows the NP correction factors obtained for the numerator (upper left) and denominator (upper right) of the $R_{\Delta\phi}(p_T)$ observable. The lower panels show the final NP correction factors C^{NP} (blue line) for $R_{\Delta\phi}(p_T)$. The red band is constructed from the envelope of individual ratios and represents the relevant uncertainties, which are less than 1%.

To further improve the accuracy, in particular at large jet p_T, the theoretical predictions are complemented with electroweak (EW) corrections. The complete set of NLO corrections for three-jet production at the LHC is presented in Ref. [82]. To obtain the EW corrections for the $R_{\Delta\phi}(p_T)$ observable, the SHERPA event generator [83] is used, interfaced with RECOLA [84,85]. Further details on the implementation of the above interface as well as on the method used for the subtraction of NLO EW infrared divergences are reported in Refs. [86,87], respectively. The pure NLO EW corrections for n-jet production are defined as:

$$\sigma_{nj}^{NLO\ EW} = \sigma_{nj}^{LO} + \sigma_{nj}^{\Delta NLO_1}, \tag{6}$$

where σ_{nj}^{LO} is the pure LO pQCD cross section and ΔNLO_1 accounts for the virtual and real EW corrections. The additive

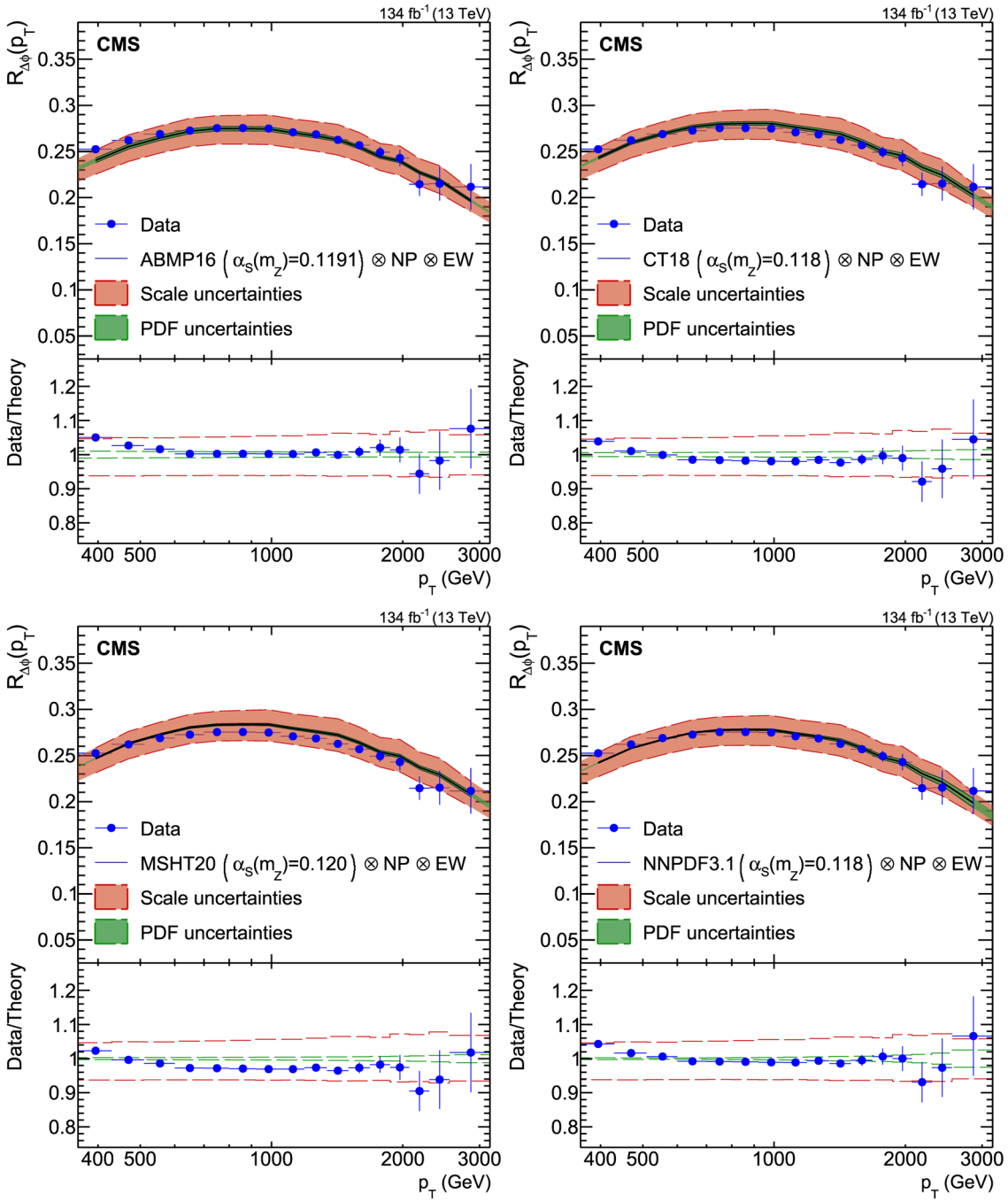

Fig. 8 The $R_{\Delta\phi}(p_{\mathrm{T}})$ observable as a function of p_{T}, compared with fixed-order theoretical calculations at NLO accuracy using the ABMP16 (upper left), CT18 (upper right), MSHT20 (lower left), and NNPDF3.1 (lower right) NLO PDF sets. The experimental data are indicated with blue dots (with error bars representing the total experimental uncertainty), the theoretical prediction for the default $\alpha_{\mathrm{S}}(m_{\mathrm{Z}})$ for each PDF set with black solid lines, the scale uncertainties with red bands, and the PDF uncertainties with green bands. The lower panel of each plot shows the ratio between experimental data and theoretical predictions

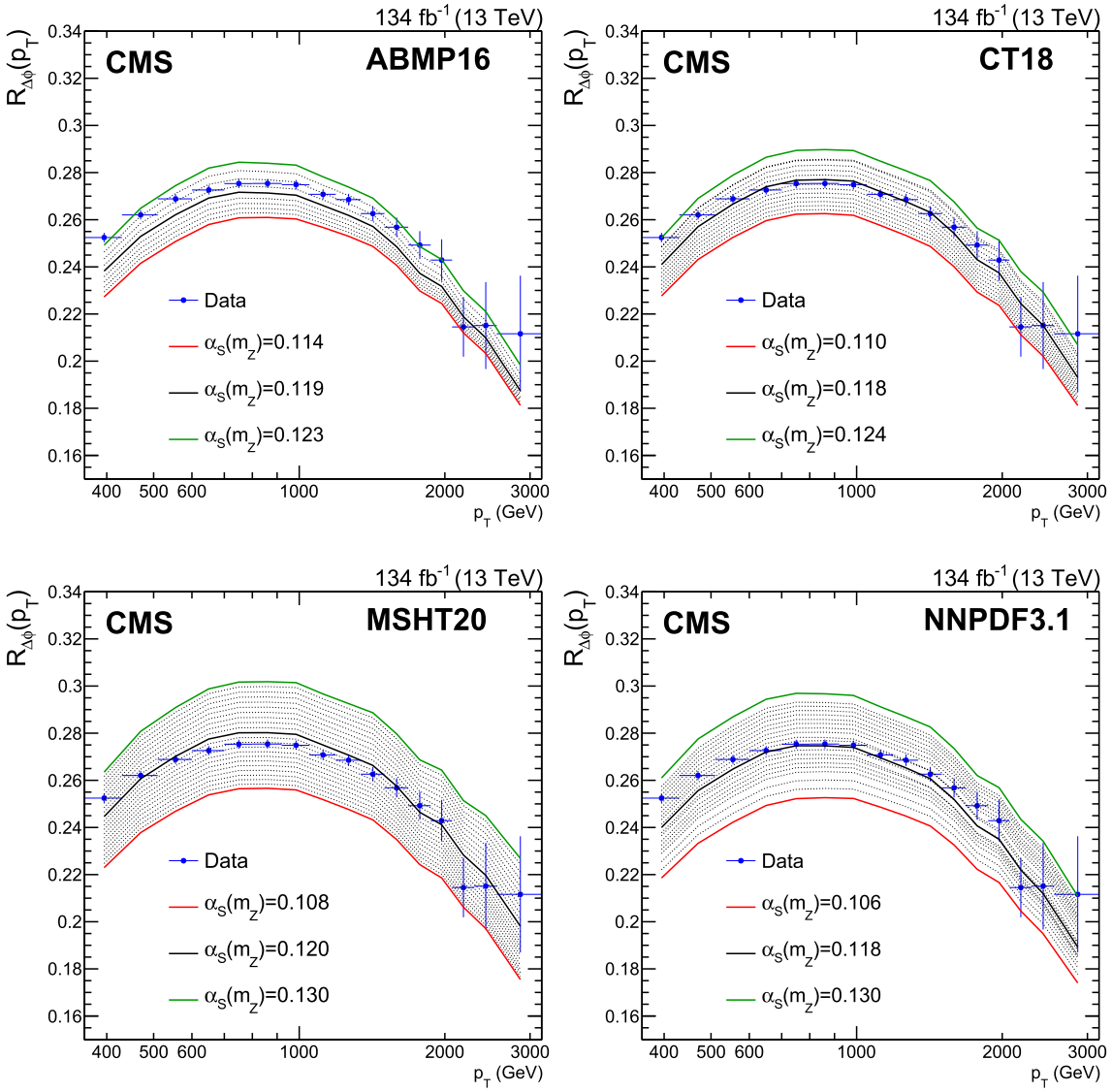

Fig. 9 Sensitivity of the $R_{\Delta\phi}(p_{\mathrm{T}})$ ratio to the strong coupling constant $\alpha_{\mathrm{S}}(m_{\mathrm{Z}})$. The data are indicated with blue dots with error bars representing the total experimental uncertainty. In each plot, the lines represent fixed-order NLO theoretical calculations obtained with ABMP16 (upper left), CT18 (upper right), MSHT20 (lower left) and NNPDF3.1 (lower right) NLO PDF sets. Solid green (red) lines indicate maximum (minimum) values, and dotted black lines intermediate values of $\alpha_{\mathrm{S}}(m_{\mathrm{Z}})$ for each PDF set

and multiplicative combination of the above corrections to the cross sections are defined, respectively, as:

$$\sigma_{\mathrm{nj}}^{\mathrm{NLO\ QCD+EW}} = \sigma_{\mathrm{nj}}^{\mathrm{LO}} + \sigma_{\mathrm{nj}}^{\Delta\mathrm{NLO}_0} + \sigma_{\mathrm{nj}}^{\Delta\mathrm{NLO}_1}, \tag{7}$$

$$\sigma_{\mathrm{nj}}^{\mathrm{NLO\ QCD\times EW}} = \sigma_{\mathrm{nj}}^{\mathrm{LO}} \left(1+\frac{\sigma_{\mathrm{nj}}^{\Delta\mathrm{NLO}_0}}{\sigma_{\mathrm{nj}}^{\mathrm{LO}}}\right)\left(1+\frac{\sigma_{\mathrm{nj}}^{\Delta\mathrm{NLO}_1}}{\sigma_{\mathrm{nj}}^{\mathrm{LO}}}\right), \tag{8}$$

where $\Delta\mathrm{NLO}_0$ accounts for the virtual and real QCD corrections. Figure 7 shows the EW corrections obtained for the numerator and denominator cross sections, and for the $R_{\Delta\phi}(p_{\mathrm{T}})$ ratio. The multiplicative combination, Eq. (8), is considered as the main result, whereas the additive combination, Eq. (7) is used as an uncertainty estimate. The relative change of the central $\alpha_{\mathrm{S}}(m_{\mathrm{Z}})$ result (Sect. 6), when the additive combination is used as the main result, is smaller than 0.2%. The EW corrections for $R_{\Delta\phi}(p_{\mathrm{T}})$ observable range from 0.2 to 5.0% and their relevant uncertainties from 0.01 to 0.53%.

Comparisons between the measurement and the theoretical predictions for the four different PDF sets are shown in Fig. 8. The PDF uncertainties in the $R_{\Delta\phi}(p_{\mathrm{T}})$ predictions are evaluated at 68% confidence level for each PDF set following either the Hessian [88] or the MC [89] methods, and are about 1–2% in all cases. The scale uncertainties in $R_{\Delta\phi}(p_{\mathrm{T}})$

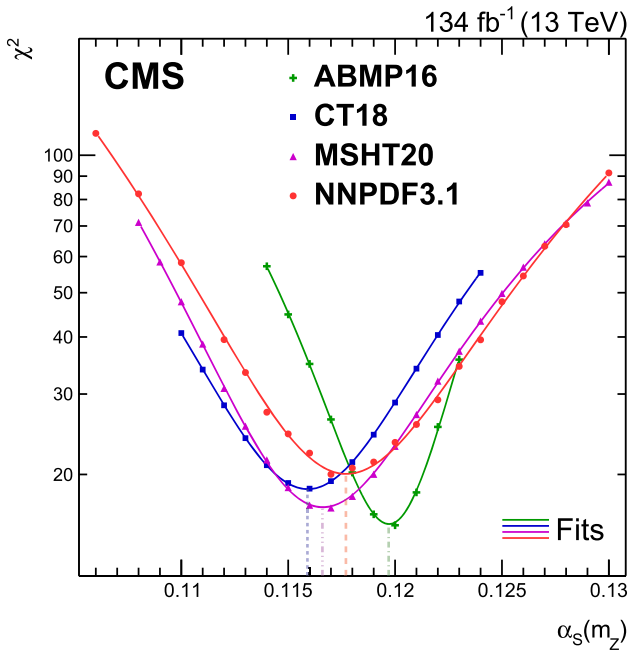

Fig. 10 Minimization of the χ^2 between experimental measurements and theoretical predictions for the $R_{\Delta\phi}(p_T)$ ratio, with respect to $\alpha_S(m_Z)$ for the ABMP16, CT18, MSHT20, and NNPDF3.1 NLO PDF sets. In this plot, only experimental uncertainties are included in the covariance matrix. The minimum value of $\alpha_S(m_Z)$ found for each PDF set is indicated with a dashed line and corresponds to the central result. The experimental uncertainty is estimated from the $\alpha_S(m_Z)$ values for which the χ^2 is increased by one unit with respect to the minimum value

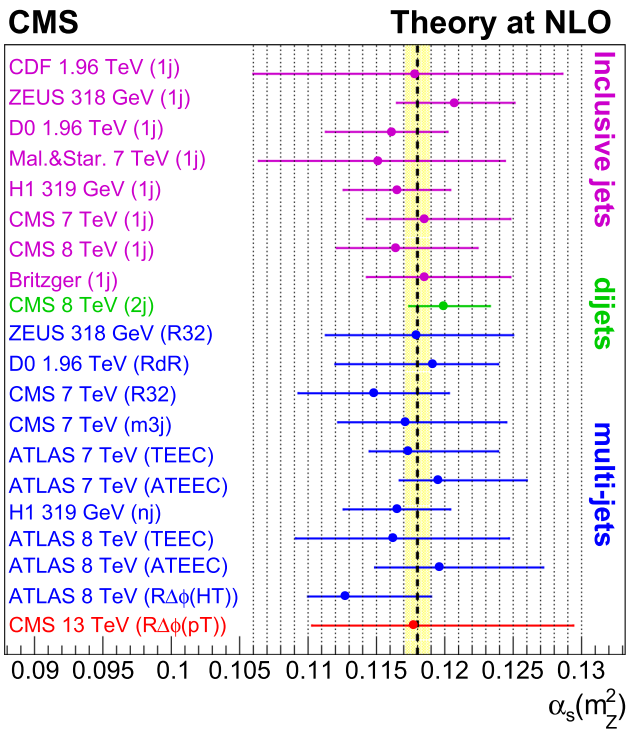

Fig. 11 Determination of $\alpha_S(m_Z)$ from the $R_{\Delta\phi}(p_T)$ ratio with the NNPDF3.1 PDF set (red), in comparison with previous NLO determinations of $\alpha_S(m_Z)$ from inclusive jet (magenta), dijet (green), and multijet (blue) measurements. The horizontal error bars indicate the total uncertainty (experimental and theoretical). The world-average $\alpha_S(m_Z)$ value is represented by the vertical dashed black line and its uncertainty by the yellow band

predictions are dominant, ranging from 2 to 8%. In general, all predictions (based on the default $\alpha_S(m_Z)$ for each PDF set) are in agreement with the measurement within the experimental and theoretical uncertainties.

6 Determination of $\alpha_S(m_Z)$

The sensitivity of the $R_{\Delta\phi}(p_T)$ ratio to the strong coupling constant is investigated by varying $\alpha_S(m_Z)$ for each PDF set within the ranges presented in Table 3. The $\alpha_S(m_Z)$ value in the fixed-order matrix elements calculations is also adjusted accordingly. Figure 9 shows the results for each PDF set, where the solid green (red) curves represent the maximum (minimum) $\alpha_S(m_Z)$ values, and the dashed black curves correspond to intermediate $\alpha_S(m_Z)$ values in $\Delta\alpha_S(m_Z) = \pm 0.001$ or $\Delta\alpha_S(m_Z) = \pm 0.002$ steps. A large sensitivity of $R_{\Delta\phi}(p_T)$ to variations of the strong coupling constant is observed for all PDF sets, and hence $R_{\Delta\phi}(p_T)$ can be used for the determination of $\alpha_S(m_Z)$.

The value of $\alpha_S(m_Z)$ is determined by minimising the goodness-of-fit (χ^2) between the experimental measurements and the theoretical predictions. The χ^2 is defined as:

$$\chi^2 = \sum_{ij}^{N} (D_i - T_i) C_{ij}^{-1} (D_j - T_j), \tag{9}$$

where N is the number of measurements, D_i are the experimental measurements, T_i are the theoretical predictions and C_{ij} is the covariance matrix, which is composed of:

$$C = C_{\text{stat}} + C_{\text{uncor}} + \left(\sum_{\text{sources}} C_{\text{JES}} \right) + C_{\text{unfold}} + C_{\text{pref}} + C_{\text{NP}} + C_{\text{PDF}} + C_{\text{EW}}, \tag{10}$$

where C_{stat} represents the statistical uncertainty, C_{uncor} is the numerical precision of the fixed-order predictions, which is assigned as uncorrelated uncertainty to each bin, C_{JES} is the systematic uncertainty for each JES uncertainty source, $C_{\text{unfold}} = C_{\text{JER}} + C_{\text{PU}} + C_{\text{MC}_{\text{model}}}$ is the systematic uncertainty induced through unfolding (representing the JER, pileup, and model uncertainties, respectively, described in Sect. 4.4), C_{pref} is the trigger prefiring uncertainty [45], and C_{NP}, C_{PDF}, and C_{EW} are the NP, PDF, and EW uncertainties, respectively.

Table 4 Results for $\alpha_S(m_Z)$, associated uncertainties, and goodness-of-fit per degree of freedom (χ^2/n_{dof}), obtained from the measured $R_{\Delta\phi}(p_T)$ distribution compared with theoretical predictions using different NLO PDF sets

NLO PDF set	$\alpha_S(m_Z)$	Exp.	NP	PDF	EW	Scale	χ^2/n_{dof}
ABMP16	0.1197	0.0008	0.0007	0.0007	0.0002	$^{+0.0043}_{-0.0042}$	16/16
CT18	0.1159	0.0013	0.0009	0.0014	0.0002	$^{+0.0099}_{-0.0067}$	19/16
MSHT20	0.1166	0.0013	0.0008	0.0010	0.0003	$^{+0.0112}_{-0.0063}$	17/16
NNPDF3.1	0.1177	0.0013	0.0011	0.0010	0.0003	$^{+0.0114}_{-0.0068}$	20/16

The JES, unfolding, prefiring, NP, PDF, and EW uncertainties are considered as 100% correlated among p_T bins, and are treated as multiplicative. Including only the experimental (statistical, JES, unfolding, and prefiring) uncertainties in the covariance matrix composition, the central $\alpha_S(m_Z)$ result is obtained by minimising the χ^2 with respect to $\alpha_S(m_Z)$. The associated experimental uncertainty is estimated from the $\alpha_S(m_Z)$ values, for which the χ^2 is increased by one unit with respect to the minimum value. Figure 10 illustrates the χ^2 minimization curves for each PDF set, which result in the $\alpha_S(m_Z)$ values and their respective experimental uncertainties listed in Table 4.

The propagation of NP, PDF, and EW uncertainties is estimated separately by repeating the χ^2 minimization procedure after including the relevant terms in Eq. (10). For the evaluation of scale uncertainties, the χ^2 comparison between measurement and theoretical predictions is repeated for the six different combinations of μ_R and μ_F scales described in Sect. 5. The up/down scale uncertainties correspond to the difference between the highest/lowest and the nominal $\alpha_S(m_Z)$ values, respectively. All resulting $\alpha_S(m_Z)$ values for the different PDF sets are fully compatible among each other, as well as with the world average [5]. The spread of these $\alpha_S(m_Z)$ values from the different PDF sets shown in Table 4, is used for the assignment of an additional uncertainty in the final $\alpha_S(m_Z)$ result due to the PDF choice. This uncertainty is evaluated from the maximum difference among the $\alpha_S(m_Z)$ values determined using the NNPDF3.1 NLO PDF set, and all the other $\alpha_S(m_Z)$ values determined using the other PDF sets shown in Table 4. The final result from the present analysis using the NNPDF3.1 NLO PDF set is: $\alpha_S(m_Z) = 0.1177^{+0.0114}_{-0.0068}$ (scale) $\pm$ 0.0013 (exp) $\pm$ 0.0011 (NP) $\pm$ 0.0010 (PDF) $\pm$ 0.0003 (EW) $\pm$ 0.0020 (PDF choice). This result, in comparison with a selection of $\alpha_S(m_Z)$ determinations at NLO accuracy obtained from inclusive jet [7,13,15,20,24,90–92], dijet [25], and multijet [7,9,16,17,19,23,91,93–95] measurements is presented in Fig. 11.

For the investigation of the running of the strong coupling, the fitted region of p_T = 360–3170 GeV (16 points) is split into four p_T subregions: 360–700, 700–1190, 1190–1870, and 1870–3170 GeV (4 points each). The fitting procedure is repeated and the $\alpha_S(m_Z)$ and all the relevant uncertainties are determined in each subregion separately. The $\alpha_S(m_Z)$ values from each subregion are evolved to $\alpha_S(Q)$, where Q is chosen as the jet p_T and is calculated as a cross-section-weighted average ($\langle Q \rangle$) for each subregion. This study is performed using the NNPDF3.1 NLO PDF set. The values of $\alpha_S(m_Z)$ and the results for $\alpha_S(Q)$ evaluated at the respective $\langle Q \rangle$ for each fitted subregion are shown in Table 5.

Figure 12 shows the energy dependence predicted by the RGE (dashed line) using the current world-average value $\alpha_S(m_Z) = 0.1180 \pm 0.0009$ [5] together with its associated total uncertainty (yellow band). The results from the $\alpha_S(Q)$ determinations in the four subregions presented in Table 5 are also shown, along with α_S values determined at lower scales by the H1 [91,94,95], ZEUS [96], D0 [7,14], CMS [16,19,20,24], and ATLAS [9,23] Collaborations. All results reported in this study are consistent with the energy dependence predicted by the RGE, and no deviation is observed from the expected behaviour up to $\sim$ 2 TeV.

7 Summary

A measurement of the $R_{\Delta\phi}(p_T)$ ratio, sensitive to azimuthal correlations in multijet events, has been presented using proton-proton collision data collected by the CMS experiment at a centre-of-mass energy of 13 TeV and corresponding to an integrated luminosity of 134 fb^{-1}. The experimental data are compared with predictions from Monte Carlo (MC) event generators, PYTHIA8 with tunes CUETP8M1 and CUETP8M2, HERWIG++ with tune UE-EE-5-CTEQ6L1, and POWHEG interfaced with each one of them. Deviations between data and MC predictions are observed in all cases, except for PYTHIA8 tune CUETP8M2, which gives a good overall description of the measurement.

The measurement is also compared with fixed-order perturbative quantum chromodynamics (pQCD) predictions at next-to-leading-order (NLO) accuracy using the NLOJET++ package within the FASTNLO framework. Those predictions are extracted for four different NLO parton distribution function (PDF) sets, ABMP16, CT18, MSHT20, and NNPDF3.1. Corrections for nonperturbative (NP) effects are evaluated using all the aforementioned MC event generators,

Table 5 Values of $\alpha_S(m_Z)$ and $\alpha_S(Q)$ determined in four different jet p_T fitting subregions corresponding to an average scale $\langle Q \rangle$ over each p_T interval

p_T range (GeV)	$\alpha_S(m_Z)$	$\langle Q \rangle$ (GeV)	$\alpha_S(Q)$
360–700	$0.1177^{+0.0104}_{-0.0067}$	433.0	$0.0967^{+0.0066}_{-0.0044}$
700–1190	$0.1162^{+0.0108}_{-0.0073}$	819.0	$0.0878^{+0.0060}_{-0.0042}$
1190–1870	$0.1159^{+0.0112}_{-0.0077}$	1346.0	$0.0830^{+0.0055}_{-0.0040}$
1870–3170	$0.1118^{+0.0110}_{-0.0070}$	2081.0	$0.0775^{+0.0051}_{-0.0034}$

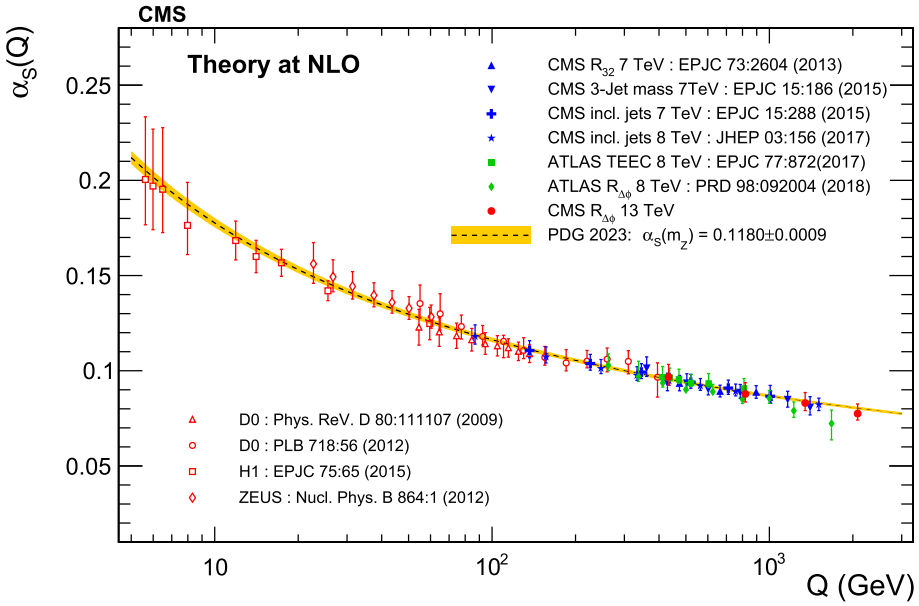

Fig. 12 Running of the strong coupling $\alpha_S(Q)$ (dashed line) evolved using the current world-average value $\alpha_S(m_Z) = 0.1180 \pm 0.0009$ [5] together with its associated total uncertainty (yellow band). The four new extractions from the present analysis (Table 5) are shown as filled red circles, compared with results from the H1 [91,94,95], ZEUS [96], D0 [7,14], CMS [16,19,20,24], and ATLAS [9,23] experiments. The vertical error bars indicate the total uncertainty (experimental and theoretical). All the experimental results shown in this figure are based on fixed-order predictions at NLO accuracy in pQCD

and are applied to the fixed-order predictions. The predictions are additionally corrected for electroweak (EW) effects that become important at large jet transverse momenta. Generally, the fixed-order predictions are in agreement with the experimental data in the phase space of this analysis, and they provide a good description of the measured $R_{\Delta\phi}(p_T)$ distribution for all PDF sets.

Based on a comparison of the measured $R_{\Delta\phi}(p_T)$ distribution and the theoretical predictions, the strong coupling at the scale of the Z boson mass is: $\alpha_S(m_Z) = 0.1177^{+0.0114}_{-0.0068}\,(\text{scale}) \pm 0.0013\,(\text{exp}) \pm 0.0011\,(\text{NP}) \pm 0.0010\,(\text{PDF}) \pm 0.0003\,(\text{EW}) \pm 0.0020\,(\text{PDF choice}) = 0.1177^{+0.0117}_{-0.0074}$, using calculations based on the NNPDF3.1 NLO PDF set. Alternative $\alpha_S(m_Z)$ results obtained with other PDF sets are compatible among each other, as well as with the central result of this work, and with the current world average, $\alpha_S(m_Z) = 0.1180 \pm 0.0009$. The spread of the $\alpha_S(m_Z)$ values obtained from different PDF sets is used for the assignment of the "PDF choice" uncertainty quoted in the final strong coupling constant derived here. The dominant uncertainty in this measurement originates from the scale dependence of the NLO pQCD predictions, and is expected to be significantly reduced with the future inclusion of fixed-order predictions at next-to-NLO accuracy.

The evolution of the strong coupling as a function of the energy scale, $\alpha_S(Q)$, has been tested up to $Q \approx 2$ TeV, a higher scale than that probed in previous H1, ZEUS, D0, CMS, and ATLAS measurements. This test has been performed by choosing as energy scale Q the average jet transverse momentum in the different intervals considered, and no deviation from the expected NLO pQCD running of the strong coupling is observed.

Acknowledgements We thank Max Reyer, Marek Schönherr and Steffen Schumann for providing the electroweak corrections for the $R_{\Delta\phi}(p_T)$ observable within the SHERPA framework. We congratulate our colleagues in the CERN accelerator departments for the excellent performance of the LHC and thank the technical and administrative staffs at CERN and at other CMS institutes for their contributions to the success of the CMS effort. In addition, we gratefully acknowledge the computing centres and personnel of the Worldwide LHC Computing Grid and other centres for delivering so effectively the computing infrastructure essential to our analyses. Finally, we acknowledge the enduring support for the construction and operation of the LHC, the CMS detector, and the supporting computing infrastructure provided by the following funding agencies: SC (Armenia), BMBWF and FWF (Austria); FNRS and FWO (Belgium); CNPq, CAPES, FAPERJ, FAPERGS, and FAPESP (Brazil); MES and BNSF (Bulgaria); CERN; CAS, MoST, and NSFC (China); MINCIENCIAS (Colombia); MSES and CSF (Croatia); RIF (Cyprus); SENESCYT (Ecuador); ERC PRG, RVTT3 and MoER TK202 (Estonia); Academy of Finland, MEC, and HIP (Finland); CEA and CNRS/IN2P3 (France); SRNSF (Georgia); BMBF, DFG, and HGF (Germany); GSRI (Greece); NKFIH (Hungary); DAE and DST (India); IPM (Iran); SFI (Ireland); INFN (Italy); MSIP and NRF (Republic of Korea); MES (Latvia); LMTLT (Lithuania); MOE and UM (Malaysia); BUAP, CINVESTAV, CONACYT, LNS, SEP, and UASLP-FAI (Mexico); MOS (Montenegro); MBIE

(New Zealand); PAEC (Pakistan); MES and NSC (Poland); FCT (Portugal); MESTD (Serbia); MCIN/AEI and PCTI (Spain); MOSTR (Sri Lanka); Swiss Funding Agencies (Switzerland); MST (Taipei); MHESI and NSTDA (Thailand); TUBITAK and TENMAK (Turkey); NASU (Ukraine); STFC (United Kingdom); DOE and NSF (USA). Individuals have received support from the Marie-Curie programme and the European Research Council and Horizon 2020 Grant, contract Nos. 675440, 724704, 752730, 758316, 765710, 824093, 101115353,101002207, and COST Action CA16108 (European Union); the Leventis Foundation; the Alfred P. Sloan Foundation; the Alexander von Humboldt Foundation; the Science Committee, project no. 22rl-037 (Armenia); the Belgian Federal Science Policy Office; the Fonds pour la Formation à la Recherche dans l'Industrie et dans l'Agriculture (FRIA-Belgium); the Agentschap voor Innovatie door Wetenschap en Technologie (IWT-Belgium); the F.R.S.-FNRS and FWO (Belgium) under the "Excellence of Science – EOS" – be.h project n. 30820817; the Beijing Municipal Science & Technology Commission, No. Z191100007219010 and Fundamental Research Funds for the Central Universities (China); the Ministry of Education, Youth and Sports (MEYS) of the Czech Republic; the Shota Rustaveli National Science Foundation, grant FR-22-985 (Georgia); the Deutsche Forschungsgemeinschaft (DFG), under Germany's Excellence Strategy – EXC 2121 "Quantum Universe" – 390833306, and under project number 400140256 - GRK2497; the Hellenic Foundation for Research and Innovation (HFRI), Project Number 2288 (Greece); the Hungarian Academy of Sciences, the New National Excellence Program - ÚNKP, the NKFIH research grants K 131991, K 133046, K 138136, K 143460, K 143477, K 146913, K 146914, K 147048, 2020-2.2.1-ED-2021-00181, and TKP2021-NKTA-64 (Hungary); the Council of Science and Industrial Research, India; ICSC – National Research Centre for High Performance Computing, Big Data and Quantum Computing and FAIR – Future Artificial Intelligence Research, funded by the EU NexGeneration program (Italy); the Latvian Council of Science; the Ministry of Education and Science, project no. 2022/WK/14, and the National Science Center, contracts Opus 2021/41/B/ST2/01369 and 2021/43/B/ST2/01552 (Poland); the Fundação para a Ciência e a Tecnologia, grant CEECIND/01334/2018 (Portugal); the National Priorities Research Program by Qatar National Research Fund; MCIN/AEI/10.13039/501100011033, ERDF "a way of making Europe", and the Programa Estatal de Fomento de la Investigación Científica y Técnica de Excelencia María de Maeztu, grant MDM-2017-0765 and Programa Severo Ochoa del Principado de Asturias (Spain); the Chulalongkorn Academic into Its 2nd Century Project Advancement Project, and the National Science, Research and Innovation Fund via the Program Management Unit for Human Resources & Institutional Development, Research and Innovation, grant B37G660013 (Thailand); the Kavli Foundation; the Nvidia Corporation; the SuperMicro Corporation; the Welch Foundation, contract C-1845; and the Weston Havens Foundation (USA).

Data Availability Statement Data cannot be made available for reasons disclosed in the data availability statement. [Authors' comment: Release and preservation of data used by the CMS Collaboration as the basis for publications https://cms-docdb.cern.ch/cgi-bin/PublicDocDB/RetrieveFile?docid=6032&filename=CMSDataPolicyV1.2.pdf&version=2 CMS data preservation, re-use and open access policy.]

Code Availability Statement This manuscript has associated code/software in a data repository. [Authors'comment: The CMS core software is publicly available on GitHub (https://github.com/cms-sw/cmssw).]

Declarations

Conflict of interest The authors declare that they have no conflict of interest.

Funded by SCOAP[3].

References

1. C.G. Callan Jr., Broken scale invariance in scalar field theory. Phys. Rev. D **2**, 1541 (1970). https://doi.org/10.1103/PhysRevD.2.1541
2. K. Symanzik, Small distance behavior in field theory and power counting. Commun. Math. Phys. **18**, 227 (1970). https://doi.org/10.1007/BF01649434
3. K. Symanzik, Small distance behavior analysis and Wilson expansion. Commun. Math. Phys. **23**, 49 (1971). https://doi.org/10.1007/BF01877596
4. P.A. Baikov, K.G. Chetyrkin, J.H. Kühn, Five-loop running of the QCD coupling constant. Phys. Rev. Lett. **118**, 082002 (2017). https://doi.org/10.1103/PhysRevLett.118.082002. arXiv:1606.08659
5. Particle Data Group, R.L. Workman et al., Review of particle physics. Prog. Theor. Exp. Phys. **2022**, 083C01 (2022). https://doi.org/10.1093/ptep/ptac097
6. D. d'Enterria et al., The strong coupling constant: state of the art and the decade ahead. J. Phys. G (2022). arXiv:2203.08271
7. D0 Collaboration, Measurement of angular correlations of jets at $\sqrt{s} = 1.96$ TeV and determination of the strong coupling at high momentum transfers. Phys. Lett. B **718**, 56 (2012). https://doi.org/10.1016/j.physletb.2012.10.003. arXiv:1207.4957
8. M. Wobisch et al., A new quantity for studies of dijet azimuthal decorrelations. JHEP **01**, 172 (2013). https://doi.org/10.1007/JHEP01(2013)172. arXiv:1211.6773
9. ATLAS Collaboration, Measurement of dijet azimuthal decorrelations in pp collisions at $\sqrt{s} = 8$ TeV with the ATLAS detector and determination of the strong coupling. Phys. Rev. D **98**, 092004 (2018). https://doi.org/10.1103/PhysRevD.98.092004. arXiv:1805.04691
10. CMS Collaboration, Precision luminosity measurement in proton-proton collisions at $\sqrt{s} = 13$ TeV in 2015 and 2016 at CMS. Eur. Phys. J. C **81**, 800 (2021). https://doi.org/10.1140/epjc/s10052-021-09538-2. arXiv:2104.01927
11. CMS Collaboration, CMS luminosity measurement for the 2017 data-taking period at $\sqrt{s} = 13$ TeV. CMS Physics Analysis Summary CMS-PAS-LUM-17-004 (2018). https://cds.cern.ch/record/2621960/
12. CMS Collaboration, CMS luminosity measurement for the 2018 data-taking period at $\sqrt{s} = 13$ TeV. CMS Physics Analysis Summary CMS-PAS-LUM-18-002 (2019). https://cds.cern.ch/record/2676164/
13. CDF Collaboration, Measurement of the strong coupling constant from inclusive jet production at the Tevatron $\bar{p}p$ collider. Phys. Rev. Lett. **88**, 042001 (2002). https://doi.org/10.1103/PhysRevLett.88.042001. arXiv:hep-ex/0108034
14. D0 Collaboration, Determination of the strong coupling constant from the inclusive jet cross section in $p\bar{p}$ collisions at $\sqrt{s} = 1.96$

TeV. Phys. Rev. D **80**, 111107 (2009). https://doi.org/10.1103/PhysRevD.80.111107. arXiv:0911.2710
15. B. Malaescu, P. Starovoitov, Evaluation of the strong coupling constant α_s using the ATLAS inclusive jet cross-section data. Eur. Phys. J. C **72**, 2041 (2012). https://doi.org/10.1140/epjc/s10052-012-2041-y. arXiv:1203.5416
16. CMS Collaboration, Measurement of the ratio of the inclusive 3-jet cross section to the inclusive 2-jet cross section in pp collisions at $\sqrt{s} = 7$ TeV and first determination of the strong coupling constant in the TeV range. Eur. Phys. J. C **73**, 2604 (2013). https://doi.org/10.1140/epjc/s10052-013-2604-6. arXiv:1304.7498
17. ATLAS Collaboration, Measurement of transverse energy-energy correlations in multi-jet events in pp collisions at $\sqrt{s} = 7$ TeV using the ATLAS detector and determination of the strong coupling constant $\alpha_s(m_Z)$. Phys. Lett. B **750**, 427 (2015). https://doi.org/10.1016/j.physletb.2015.09.050. arXiv:1508.01579
18. CMS Collaboration, Determination of the top-quark pole mass and strong coupling constant from the $t\bar{t}$ production cross section in pp collisions at $\sqrt{s} = 7$ TeV. Phys. Lett. B **728**, 496 (2014). https://doi.org/10.1016/j.physletb.2013.12.009. arXiv:1307.1907. [Erratum: https://doi.org/10.1016/j.physletb.2014.08.040]
19. CMS Collaboration, Measurement of the inclusive 3-jet production differential cross section in proton-proton collisions at 7 TeV and determination of the strong coupling constant in the TeV range. Eur. Phys. J. C **75**, 186 (2015). https://doi.org/10.1140/epjc/s10052-015-3376-y. arXiv:1412.1633
20. CMS Collaboration, Constraints on parton distribution functions and extraction of the strong coupling constant from the inclusive jet cross section in pp collisions at $\sqrt{s} = 7$ TeV. Eur. Phys. J. C **75**, 288 (2015). https://doi.org/10.1140/epjc/s10052-015-3499-1. arXiv:1410.6765
21. CMS Collaboration, Determination of the strong coupling constant $\alpha_S(m_Z)$ from measurements of inclusive $W^{\pm}$ and Z boson production cross sections in proton-proton collisions at $\sqrt{s} = 7$ and 8 TeV. JHEP **06**, 018 (2020). https://doi.org/10.1007/JHEP06(2020)018. arXiv:1912.04387
22. D. d'Enterria, A. Poldaru, Extraction of the strong coupling $\alpha_S(m_Z)$ from a combined NNLO analysis of inclusive electroweak boson cross sections at hadron colliders. JHEP **06**, 016 (2020). https://doi.org/10.1007/JHEP06(2020)016. arXiv:1912.11733
23. ATLAS Collaboration, Determination of the strong coupling constant α_s from transverse energy-energy correlations in multijet events at $\sqrt{s} = 8$ TeV using the ATLAS detector. Eur. Phys. J. C **77**, 872 (2017). https://doi.org/10.1140/epjc/s10052-017-5442-0. arXiv:1707.02562
24. CMS Collaboration, Measurement and QCD analysis of double-differential inclusive jet cross sections in pp collisions at $\sqrt{s} = 8$ TeV and cross section ratios to 2.76 and 7 TeV. JHEP **03**, 156 (2017). https://doi.org/10.1007/JHEP03(2017)156. arXiv:1609.05331
25. CMS Collaboration, Measurement of the triple-differential dijet cross section in proton-proton collisions at $\sqrt{s} = 8$ TeV and constraints on parton distribution functions. Eur. Phys. J. C **77**, 746 (2017). https://doi.org/10.1140/epjc/s10052-017-5286-7. arXiv:1705.02628
26. CMS Collaboration, Measurement of jet substructure observables in $t\bar{t}$ events from proton-proton collisions at $\sqrt{s} = 13$ TeV. Phys. Rev. D **98**, 092014 (2018). https://doi.org/10.1103/PhysRevD.98.092014. arXiv:1808.07340
27. CMS Collaboration, Measurement of the $t\bar{t}$ production cross section, the top quark mass, and the strong coupling constant using dilepton events in pp collisions at $\sqrt{s} = 13$ TeV. Eur. Phys. J. C **79**, 368 (2019). https://doi.org/10.1140/epjc/s10052-019-6863-8. arXiv:1812.10505
28. CMS Collaboration, Measurement of $t\bar{t}$ normalised multi-differential cross sections in pp collisions at $\sqrt{s} = 13$ TeV, and simultaneous determination of the strong coupling strength, top quark pole mass, and parton distribution functions. Eur. Phys. J. C **80**, 658 (2020). https://doi.org/10.1140/epjc/s10052-020-7917-7. arXiv:1904.05237
29. ATLAS Collaboration, Determination of the strong coupling constant from transverse energy-energy correlations in multijet events at $\sqrt{s} = 13$ TeV with the ATLAS detector. JHEP **07**, 085 (2023). https://doi.org/10.1007/JHEP07(2023)085. arXiv:2301.09351
30. CMS Collaboration, Measurement and QCD analysis of double-differential inclusive jet cross sections in proton-proton collisions at $\sqrt{s} = 13$ TeV. JHEP **02**, 142 (2022). https://doi.org/10.1007/JHEP02(2022)142. arXiv:2111.10431. [Addendum: https://doi.org/10.1007/JHEP12(2022)035]
31. CMS Collaboration, Measurement of multidifferential cross sections for dijet production in proton-proton collisions at $\sqrt{s} =$ 13 TeV. Eur. Phys. J. C (2023). arXiv:2312.16669
32. CMS Collaboration, Measurement of energy correlators inside jets and determination of the strong coupling $\alpha_S(m_Z)$. Phys. Rev. Lett. (2024). arXiv:2402.13864
33. HEPData record for this analysis, (2024). https://doi.org/10.17182/hepdata.150596
34. CMS Collaboration, The CMS experiment at the CERN LHC. JINST **3**, S08004 (2008). https://doi.org/10.1088/1748-0221/3/08/S08004
35. CMS Collaboration, Performance of the CMS level-1 trigger in proton-proton collisions at $\sqrt{s} = 13$ TeV. JINST **15**, P10017 (2020). https://doi.org/10.1088/1748-0221/15/10/P10017. arXiv:2006.10165
36. CMS Collaboration, The CMS trigger system. JINST **12**, P01020 (2017). https://doi.org/10.1088/1748-0221/12/01/P01020. arXiv:1609.02366
37. CMS Collaboration, Particle-flow reconstruction and global event description with the CMS detector. JINST **12**, P10003 (2017). https://doi.org/10.1088/1748-0221/12/10/P10003. arXiv:1706.04965
38. CMS Collaboration, Technical proposal for the Phase-II upgrade of the Compact Muon Solenoid, CMS Technical Proposal CERN-LHCC-2015-010, CMS-TDR-15-02 (2015). http://cds.cern.ch/record/2020886
39. M. Cacciari, G.P. Salam, G. Soyez, The anti-k_T jet clustering algorithm. JHEP **04**, 063 (2008). https://doi.org/10.1088/1126-6708/2008/04/063. arXiv:0802.1189
40. M. Cacciari, G.P. Salam, G. Soyez, FastJet user manual. Eur. Phys. J. C **72**, 1896 (2012). https://doi.org/10.1140/epjc/s10052-012-1896-2. arXiv:1111.6097
41. CMS Collaboration, Pileup mitigation at CMS in 13 TeV data. JINST **15**, P09018 (2020). https://doi.org/10.1088/1748-0221/15/09/P09018. arXiv:2003.00503
42. CMS Collaboration, Jet energy scale and resolution in the CMS experiment in pp collisions at 8 TeV. JINST **12**, P02014 (2017). https://doi.org/10.1088/1748-0221/12/02/P02014. arXiv:1607.03663
43. CMS Collaboration, Jet algorithms performance in 13 TeV data, CMS Physics Analysis Summary CMS-PAS-JME-16-003 (2017). https://cds.cern.ch/record/2256875
44. CMS Collaboration, Performance of missing transverse momentum reconstruction in proton-proton collisions at $\sqrt{s} = 13$ TeV using the CMS detector. JINST **14**, P07004 (2019). https://doi.org/10.1088/1748-0221/14/07/P07004. arXiv:1903.06078
45. CMS Collaboration, Performance of the CMS electromagnetic calorimeter in pp collisions at $\sqrt{s} = 13$ TeV, Technical Report CERN-EP-2024-014, CMS-EGM-18-002-003 (2024). http://cds.cern.ch/record/2892650
46. T. Sjöstrand et al., An introduction to PYTHIA 8.2. Comput. Phys. Commun. **191**, 159 (2015). https://doi.org/10.1016/j.cpc.2015.01.024. arXiv:1410.3012

47. CMS Collaboration, Event generator tunes obtained from underlying event and multiparton scattering measurements. Eur. Phys. J. C **76**, 155 (2016). https://doi.org/10.1140/epjc/s10052-016-3988-x. arXiv:1512.00815
48. CMS Collaboration, Extraction and validation of a new set of CMS PYTHIA8 tunes from underlying-event measurements. Eur. Phys. J. C **80**, 4 (2020). https://doi.org/10.1140/epjc/s10052-019-7499-4. arXiv:1903.12179
49. S. Schmitt, TUnfold: an algorithm for correcting migration effects in high energy physics. JINST **7**, T10003 (2012). https://doi.org/10.1088/1748-0221/7/10/T10003. arXiv:1205.6201
50. V. Blobel, Unfolding, ch. 6 (Wiley, 2013), p. 187. https://doi.org/10.1002/9783527653416.ch6
51. GEANT4 Collaboration, Geant4-a simulation toolkit. Nucl. Instrum. Methods A **506**, 250 (2003). https://doi.org/10.1016/S0168-9002(03)01368-8
52. J. Alwall et al., The automated computation of tree-level and next-to-leading order differential cross sections, and their matching to parton shower simulations. JHEP **07**, 079 (2014). https://doi.org/10.1007/JHEP07(2014)079. arXiv:1405.0301
53. J. Alwall et al., Comparative study of various algorithms for the merging of parton showers and matrix elements in hadronic collisions. Eur. Phys. J. C **53**, 473 (2008). https://doi.org/10.1140/epjc/s10052-007-0490-5. arXiv:0706.2569
54. M. Bähr et al., Herwig++ physics and manual. Eur. Phys. J. C **58**, 639 (2008). https://doi.org/10.1140/epjc/s10052-008-0798-9. arXiv:0803.0883
55. S. Alioli, P. Nason, C. Oleari, E. Re, A general framework for implementing NLO calculations in shower Monte Carlo programs: the POWHEG BOX. JHEP **06**, 043 (2010). https://doi.org/10.1007/JHEP06(2010)043. arXiv:1002.2581
56. C. Bierlich et al., Robust independent validation of experiment and theory: Rivet version 3. SciPost Phys. **8**, 026 (2020). https://doi.org/10.21468/SciPostPhys.8.2.026. arXiv:1912.05451
57. B.R. Webber, A QCD model for jet fragmentation including soft gluon interference. Nucl. Phys. B **238**, 492 (1984). https://doi.org/10.1016/0550-3213(84)90333-X
58. M.H. Seymour, A. Siódmok, Constraining MPI models using σ_{eff} and recent Tevatron and LHC underlying event data. JHEP **10**, 113 (2013). https://doi.org/10.1007/JHEP10(2013)113. arXiv:1307.5015
59. D. Stump et al., Inclusive jet production, parton distributions, and the search for new physics. JHEP **10**, 046 (2003). https://doi.org/10.1088/1126-6708/2003/10/046. arXiv:hep-ph/0303013
60. B. Andersson, *The Lund Model*, vol. 7 (Cambridge University Press, 2005), p. 7. https://doi.org/10.1017/CBO9780511524363
61. NNPDF Collaboration, Parton distributions with QED corrections. Nucl. Phys. B **877**, 290 (2013). https://doi.org/10.1016/j.nuclphysb.2013.10.010. arXiv:1308.0598
62. NNPDF Collaboration, Unbiased global determination of parton distributions and their uncertainties at NNLO and at LO. Nucl. Phys. B **855**, 153 (2012). https://doi.org/10.1016/j.nuclphysb.2011.09.024. arXiv:1107.2652
63. CMS Collaboration, Investigations of the impact of the parton shower tuning in Pythia 8 in the modelling of $\mathrm{t\bar{t}}$ at $\sqrt{s} = 8$ and 13 TeV. CMS Physics Analysis Summary CMS-PAS-TOP-16-021 (2016). https://cds.cern.ch/record/2235192
64. NNPDF Collaboration, Parton distributions for the LHC Run II. JHEP **04**, 040 (2015). https://doi.org/10.1007/JHEP04(2015)040. arXiv:1410.8849
65. P. Nason, A new method for combining NLO QCD with shower Monte Carlo algorithms. JHEP **11**, 040 (2004). https://doi.org/10.1088/1126-6708/2004/11/040. arXiv:hep-ph/0409146
66. S. Frixione, P. Nason, C. Oleari, Matching NLO QCD computations with parton shower simulations: the POWHEG method. JHEP **11**, 070 (2007). https://doi.org/10.1088/1126-6708/2007/11/070. arXiv:0709.2092
67. Z. Nagy, Three-jet cross sections in hadron-hadron collisions at next-to-leading order. Phys. Rev. Lett. **88**, 122003 (2002). https://doi.org/10.1103/PhysRevLett.88.122003. arXiv:hep-ph/0110315
68. Z. Nagy, Next-to-leading order calculation of three-jet observables in hadron-hadron collision. Phys. Rev. D **68**, 094002 (2003). https://doi.org/10.1103/PhysRevD.68.094002. arXiv:hep-ph/0307268
69. T. Kluge, K. Rabbertz, M. Wobisch, FastNLO: Fast pQCD calculations for PDF fits, in *14th International Workshop on Deep Inelastic Scattering*, p. 483 (2006). https://doi.org/10.1142/9789812706706_0110. arXiv:hep-ph/0609285
70. fastNLO Collaboration, D. Britzger, K. Rabbertz, F. Stober, M. Wobisch, New features in version 2 of the fastNLO project, in *20th International Workshop on Deep-Inelastic Scattering and Related Subjects*, p. 217 (2012). https://doi.org/10.3204/DESY-PROC-2012-02/165. arXiv:1208.3641
71. A. Buckley et al., LHAPDF6: parton density access in the LHC precision era. Eur. Phys. J. C **75**, 132 (2015). https://doi.org/10.1140/epjc/s10052-015-3318-8. arXiv:1412.7420
72. J. Currie et al., Infrared sensitivity of single jet inclusive production at hadron colliders. JHEP **10**, 155 (2018). https://doi.org/10.1007/JHEP10(2018)155. arXiv:1807.03692
73. M. Czakon, A. Mitov, R. Poncelet, Next-to-next-to-leading order study of three-jet production at the LHC. Phys. Rev. Lett. **127**, 152001 (2021). https://doi.org/10.1103/PhysRevLett.127.152001. arXiv:2106.05331. [Erratum: https://doi.org/10.1103/PhysRevLett.129.119901]
74. M. Alvarez et al., NNLO QCD corrections to event shapes at the LHC. JHEP **03**, 129 (2023). https://doi.org/10.1007/JHEP03(2023)129. arXiv:2301.01086
75. M. Cacciari et al., The top-antitop cross-section at 1.8 TeV and 1.96 TeV: a study of the systematics due to parton densities and scale dependence. JHEP **04**, 068 (2004). https://doi.org/10.1088/1126-6708/2004/04/068. arXiv:hep-ph/0303085
76. S. Catani, D. de Florian, M. Grazzini, P. Nason, Soft gluon resummation for Higgs boson production at hadron colliders. JHEP **07**, 028 (2003). https://doi.org/10.1088/1126-6708/2003/07/028. arXiv:hep-ph/0306211
77. A. Banfi, G.P. Salam, G. Zanderighi, Phenomenology of event shapes at hadron colliders. JHEP **06**, 038 (2010). https://doi.org/10.1007/JHEP06(2010)038. arXiv:1001.4082
78. S. Alekhin, J. Blümlein, S. Moch, R. Plačakyté, Parton distribution functions, α_s, and heavy-quark masses for LHC Run II. Phys. Rev. D **96**, 014011 (2017). https://doi.org/10.1103/PhysRevD.96.014011. arXiv:1701.05838
79. T.-J. Hou et al., New CTEQ global analysis of quantum chromodynamics with high-precision data from the LHC. Phys. Rev. D **103**, 014013 (2021). https://doi.org/10.1103/PhysRevD.103.014013. arXiv:1912.10053
80. S. Bailey et al., Parton distributions from LHC, HERA, Tevatron and fixed target data: MSHT20 PDFs. Eur. Phys. J. C **81**, 341 (2021). https://doi.org/10.1140/epjc/s10052-021-09057-0. arXiv:2012.04684
81. NNPDF Collaboration, Parton distributions from high-precision collider data. Eur. Phys. J. C **77**, 663 (2017). https://doi.org/10.1140/epjc/s10052-017-5199-5. arXiv:1706.00428
82. M. Reyer, M. Schönherr, S. Schumann, Full NLO corrections to 3-jet production and $\mathbf{R_{32}}$ at the LHC. Eur. Phys. J. C **79**, 321 (2019). https://doi.org/10.1140/epjc/s10052-019-6815-3. arXiv:1902.01763
83. Sherpa Collaboration, Event generation with Sherpa 2.2. SciPost Phys. **7**, 034 (2019). https://doi.org/10.21468/SciPostPhys.7.3.034. arXiv:1905.09127

84. S. Actis et al., Recursive generation of one-loop amplitudes in the Standard Model. JHEP **04**, 037 (2013). https://doi.org/10.1007/JHEP04(2013)037. arXiv:1211.6316
85. S. Actis et al., RECOLA: REcursive Computation of One-Loop Amplitudes. Comput. Phys. Commun. **214**, 140 (2017). https://doi.org/10.1016/j.cpc.2017.01.004. arXiv:1605.01090
86. B. Biedermann et al., Automation of NLO QCD and EW corrections with Sherpa and Recola. Eur. Phys. J. C **77**, 492 (2017). https://doi.org/10.1140/epjc/s10052-017-5054-8. arXiv:1704.05783
87. M. Schönherr, An automated subtraction of NLO EW infrared divergences. Eur. Phys. J. C **78**, 119 (2018). https://doi.org/10.1140/epjc/s10052-018-5600-z. arXiv:1712.07975
88. J. Pumplin et al., Uncertainties of predictions from parton distribution functions. 2. The Hessian method. Phys. Rev. D **65**, 014013 (2001). https://doi.org/10.1103/PhysRevD.65.014013. arXiv:hep-ph/0101032
89. W.T. Giele, S.A. Keller, D.A. Kosower, Parton distribution function uncertainties (2001). arXiv:hep-ph/0104052
90. ZEUS Collaboration, Jet-radius dependence of inclusive-jet cross-sections in deep inelastic scattering at HERA. Phys. Lett. B **649**, 12 (2007). https://doi.org/10.1016/j.physletb.2007.03.039. arXiv:hep-ex/0701039
91. H1 Collaboration, Measurement of multijet production in ep collisions at high Q^2 and determination of the strong coupling α_s. Eur. Phys. J. C **75**, 65 (2015). https://doi.org/10.1140/epjc/s10052-014-3223-6. arXiv:1406.4709
92. D. Britzger et al., Determination of the strong coupling constant using inclusive jet cross section data from multiple experiments. Eur. Phys. J. C **79**, 68 (2019). https://doi.org/10.1140/epjc/s10052-019-6551-8. arXiv:1712.00480
93. ZEUS Collaboration, Multijet production in neutral current deep inelastic scattering at HERA and determination of α_s. Eur. Phys. J. C **44**, 183 (2005). https://doi.org/10.1140/epjc/s2005-02347-1. arXiv:hep-ex/0502007
94. H1 Collaboration, Jet production in ep collisions at high Q^2 and determination of α_s. Eur. Phys. J. C **65**, 363 (2010). https://doi.org/10.1140/epjc/s10052-009-1208-7. arXiv:0904.3870
95. H1 Collaboration, Jet production in ep collisions at low Q^2 and determination of α_s. Eur. Phys. J. C **67**, 1 (2010). https://doi.org/10.1140/epjc/s10052-010-1282-x. arXiv:0911.5678
96. ZEUS Collaboration, Inclusive-jet photoproduction at HERA and determination of α_s. Nucl. Phys. B **864**, 1 (2012). https://doi.org/10.1016/j.nuclphysb.2012.06.006. arXiv:1205.6153

CMS Collaboration

Yerevan Physics Institute, Yerevan, Armenia
A. Hayrapetyan, A. Tumasyan[1]

Institut für Hochenergiephysik, Vienna, Austria
W. Adam, J. W. Andrejkovic, T. Bergauer, S. Chatterjee, K. Damanakis, M. Dragicevic, P. S. Hussain, M. Jeitler[2], N. Krammer, A. Li, D. Liko, I. Mikulec, J. Schieck[2], R. Schöfbeck, D. Schwarz, M. Sonawane, S. Templ, W. Waltenberger, C.-E. Wulz[2]

Universiteit Antwerpen, Antwerpen, Belgium
M. R. Darwish[3], T. Janssen, P. Van Mechelen

Vrije Universiteit Brussel, Brussels, Belgium
E. S. Bols, J. D'Hondt, S. Dansana, A. De Moor, M. Delcourt, H. El Faham, S. Lowette, I. Makarenko, D. Müller, A. R. Sahasransu, S. Tavernier, M. Tytgat[4], G. P. Van Onsem, S. Van Putte, D. Vannerom

Université Libre de Bruxelles, Brussels, Belgium
B. Clerbaux, A. K. Das, G. De Lentdecker, L. Favart, D. Hohov, J. Jaramillo, A. Khalilzadeh, K. Lee, M. Mahdavikhorrami, A. Malara, S. Paredes, L. Pétré, N. Postiau, L. Thomas, M. Vanden Bemden, C. Vander Velde, P. Vanlaer

Ghent University, Ghent, Belgium
M. De Coen, D. Dobur, Y. Hong, J. Knolle, L. Lambrecht, G. Mestdach, K. Mota Amarilo, C. Rendón, A. Samalan, K. Skovpen, N. Van Den Bossche, J. van der Linden, L. Wezenbeek

Université Catholique de Louvain, Louvain-la-Neuve, Belgium
A. Benecke, A. Bethani, G. Bruno, C. Caputo, C. Delaere, I. S. Donertas, A. Giammanco, K. Jaffel, Sa. Jain, V. Lemaitre, J. Lidrych, P. Mastrapasqua, K. Mondal, T. T. Tran, S. Wertz

Centro Brasileiro de Pesquisas Fisicas, Rio de Janeiro, Brazil
G. A. Alves, E. Coelho, C. Hensel, T. Menezes De Oliveira, A. Moraes, P. Rebello Teles, M. Soeiro

Universidade do Estado do Rio de Janeiro, Rio de Janeiro, Brazil
W. L. Aldá Júnior, M. Alves Gallo Pereira, M. Barroso Ferreira Filho, H. Brandao Malbouisson, W. Carvalho, J. Chinellato[5], E. M. Da Costa, G. G. Da Silveira[6], D. De Jesus Damiao, S. Fonseca De Souza, R. Gomes De Souza, J. Martins[7], C. Mora Herrera, L. Mundim, H. Nogima, A. Santoro, A. Sznajder, M. Thiel, A. Vilela Pereira

Universidade Estadual Paulista, Universidade Federal do ABC, São Paulo, Brazil
C. A. Bernardes[6], L. Calligaris, T. R. Fernandez Perez Tomei, E. M. Gregores, P. G. Mercadante, S. F. Novaes, B. Orzari, Sandra S. Padula

Institute for Nuclear Research and Nuclear Energy, Bulgarian Academy of Sciences, Sofia, Bulgaria
A. Aleksandrov, G. Antchev, R. Hadjiiska, P. Iaydjiev, M. Misheva, M. Shopova, G. Sultanov

University of Sofia, Sofia, Bulgaria
A. Dimitrov, L. Litov, B. Pavlov, P. Petkov, A. Petrov, E. Shumka

Instituto De Alta Investigación, Universidad de Tarapacá, Casilla 7 D, Arica, Chile
S. Keshri, S. Thakur

Beihang University, Beijing, China
T. Cheng, Q. Guo, T. Javaid, L. Yuan

Department of Physics, Tsinghua University, Beijing, China
Z. Hu, J. Liu, K. Yi[8,9]

Institute of High Energy Physics, Beijing, China
G. M. Chen[10], H. S. Chen[10], M. Chen[10], F. Iemmi, C. H. Jiang, A. Kapoor[11], H. Liao, Z.-A. Liu[12], R. Sharma[13], J. N. Song[12], J. Tao, C. Wang[10], J. Wang, Z. Wang[10], H. Zhang

State Key Laboratory of Nuclear Physics and Technology, Peking University, Beijing, China
A. Agapitos, Y. Ban, A. Levin, C. Li, Q. Li, Y. Mao, S. J. Qian, X. Sun, D. Wang, H. Yang, L. Zhang, C. Zhou

Sun Yat-Sen University, Guangzhou, China
Z. You

University of Science and Technology of China, Hefei, China
N. Lu

Nanjing Normal University, Nanjing, China
G. Bauer[14]

Institute of Modern Physics and Key Laboratory of Nuclear Physics and Ion-beam Application (MOE)-Fudan University, Shanghai, China
X. Gao[15], D. Leggat, H. Okawa

Zhejiang University, Hangzhou, Zhejiang, China
Z. Lin, C. Lu, M. Xiao

Universidad de Los Andes, Bogotá, Colombia
C. Avila, D. A. Barbosa Trujillo, A. Cabrera, C. Florez, J. Fraga, J. A. Reyes Vega

Universidad de Antioquia, Medellin, Colombia
J. Mejia Guisao, F. Ramirez, M. Rodriguez, J. D. Ruiz Alvarez

University of Split, Faculty of Electrical Engineering, Mechanical Engineering and Naval Architecture, Split, Croatia
D. Giljanovic, N. Godinovic, D. Lelas, A. Sculac

Faculty of Science, University of Split, Split, Croatia
M. Kovac, T. Sculac[16]

Institute Rudjer Boskovic, Zagreb, Croatia
P. Bargassa, V. Brigljevic, B. K. Chitroda, D. Ferencek, S. Mishra, A. Starodumov[17], T. Susa

University of Cyprus, Nicosia, Cyprus
A. Attikis, K. Christoforou, S. Konstantinou, J. Mousa, C. Nicolaou, F. Ptochos, P. A. Razis, H. Rykaczewski, H. Saka, A. Stepennov

Charles University, Prague, Czech Republic
M. Finger, M. Finger Jr., A. Kveton

Escuela Politecnica Nacional, Quito, Ecuador
E. Ayala

Universidad San Francisco de Quito, Quito, Ecuador
E. Carrera Jarrin

Academy of Scientific Research and Technology of the Arab Republic of Egypt, Egyptian Network of High Energy Physics, Cairo, Egypt
A. A. Abdelalim[18,19], E. Salama[20,21]

Center for High Energy Physics (CHEP-FU), Fayoum University, El-Fayoum, Egypt
M. A. Mahmoud, Y. Mohammed

National Institute of Chemical Physics and Biophysics, Tallinn, Estonia
K. Ehataht, M. Kadastik, T. Lange, S. Nandan, C. Nielsen, J. Pata, M. Raidal, L. Tani, C. Veelken

Department of Physics, University of Helsinki, Helsinki, Finland
H. Kirschenmann, K. Osterberg, M. Voutilainen

Helsinki Institute of Physics, Helsinki, Finland
S. Bharthuar, E. Brücken, F. Garcia, K. T. S. Kallonen, R. Kinnunen, T. Lampén, K. Lassila-Perini, S. Lehti, T. Lindén, L. Martikainen, M. Myllymäki, M. m. Rantanen, H. Siikonen, E. Tuominen, J. Tuominiemi

Lappeenranta-Lahti University of Technology, Lappeenranta, Finland
P. Luukka, H. Petrow

IRFU, CEA, Université Paris-Saclay, Gif-sur-Yvette, France
M. Besancon, F. Couderc, M. Dejardin, D. Denegri, J. L. Faure, F. Ferri, S. Ganjour, P. Gras, G. Hamel de Monchenault, V. Lohezic, J. Malcles, J. Rander, A. Rosowsky, M. Ö. Sahin, A. Savoy-Navarro[22], P. Simkina, M. Titov, M. Tornago

Laboratoire Leprince-Ringuet, CNRS/IN2P3, Ecole Polytechnique, Institut Polytechnique de Paris, Palaiseau, France
C. Baldenegro Barrera, F. Beaudette, A. Buchot Perraguin, P. Busson, A. Cappati, C. Charlot, F. Damas, O. Davignon, A. De Wit, B. A. Fontana Santos Alves, S. Ghosh, A. Gilbert, R. Granier de Cassagnac, A. Hakimi, B. Harikrishnan, L. Kalipoliti, G. Liu, J. Motta, M. Nguyen, C. Ochando, L. Portales, R. Salerno, J. B. Sauvan, Y. Sirois, A. Tarabini, E. Vernazza, A. Zabi, A. Zghiche

CNRS, IPHC UMR 7178, Université de Strasbourg, Strasbourg, France
J.-L. Agram[23], J. Andrea, D. Apparu, D. Bloch, J.-M. Brom, E. C. Chabert, C. Collard, S. Falke, U. Goerlach, C. Grimault, R. Haeberle, A.-C. Le Bihan, M. Meena, G. Saha, M. A. Sessini, P. Van Hove

Institut de Physique des 2 Infinis de Lyon (IP2I), Villeurbanne, France
S. Beauceron, B. Blancon, G. Boudoul, N. Chanon, J. Choi, D. Contardo, P. Depasse, C. Dozen[24], H. El Mamouni, J. Fay, S. Gascon, M. Gouzevitch, C. Greenberg, G. Grenier, B. Ille, I. B. Laktineh, M. Lethuillier, L. Mirabito, S. Perries, A. Purohit, M. Vander Donckt, P. Verdier, J. Xiao

Georgian Technical University, Tbilisi, Georgia
I. Lomidze, T. Toriashvili[25], Z. Tsamalaidze[17]

RWTH Aachen University, I. Physikalisches Institut, Aachen, Germany
V. Botta, L. Feld, K. Klein, M. Lipinski, D. Meuser, A. Pauls, N. Röwert, M. Teroerde

RWTH Aachen University, III. Physikalisches Institut A, Aachen, Germany
S. Diekmann, A. Dodonova, N. Eich, D. Eliseev, F. Engelke, J. Erdmann, M. Erdmann, P. Fackeldey, B. Fischer, T. Hebbeker, K. Hoepfner, F. Ivone, A. Jung, M. y. Lee, L. Mastrolorenzo, F. Mausolf, M. Merschmeyer, A. Meyer, S. Mukherjee, D. Noll, A. Novak, F. Nowotny, A. Pozdnyakov, Y. Rath, W. Redjeb, F. Rehm, H. Reithler, U. Sarkar, V. Sarkisovi, A. Schmidt, A. Sharma, J. L. Spah, A. Stein, F. Torres Da Silva De Araujo[26], L. Vigilante, S. Wiedenbeck, S. Zaleski

RWTH Aachen University, III. Physikalisches Institut B, Aachen, Germany
C. Dziwok, G. Flügge, W. Haj Ahmad[27], T. Kress, A. Nowack, O. Pooth, A. Stahl, T. Ziemons, A. Zotz

Deutsches Elektronen-Synchrotron, Hamburg, Germany
H. Aarup Petersen, M. Aldaya Martin, J. Alimena, S. Amoroso, Y. An, S. Baxter, M. Bayatmakou, H. Becerril Gonzalez, O. Behnke, A. Belvedere, S. Bhattacharya, F. Blekman[28], K. Borras[29], A. Campbell, A. Cardini, C. Cheng, F. Colombina, S. Consuegra Rodríguez, G. Correia Silva, M. De Silva, G. Eckerlin, D. Eckstein, L. I. Estevez Banos, O. Filatov, E. Gallo[28], A. Geiser, A. Giraldi, G. Greau, V. Guglielmi, M. Guthoff, A. Hinzmann, A. Jafari[30], L. Jeppe, N. Z. Jomhari, B. Kaech, M. Kasemann, C. Kleinwort, R. Kogler, M. Komm, D. Krücker, W. Lange, D. Leyva Pernia, K. Lipka[31], W. Lohmann[32], R. Mankel, I.-A. Melzer-Pellmann, M. Mendizabal Morentin, A. B. Meyer, G. Milella, A. Mussgiller, L. P. Nair, A. Nürnberg, Y. Otarid, J. Park, D. Pérez Adán, E. Ranken, A. Raspereza, B. Ribeiro Lopes, J. Rübenach, A. Saggio, M. Scham[29,33], S. Schnake[29], P. Schütze, C. Schwanenberger[28], D. Selivanova, K. Sharko, M. Shchedrolosiev, R. E. Sosa Ricardo, D. Stafford, F. Vazzoler, A. Ventura Barroso, R. Walsh, Q. Wang, Y. Wen, K. Wichmann, L. Wiens[29], C. Wissing, Y. Yang, A. Zimermmane Castro Santos

University of Hamburg, Hamburg, Germany
A. Albrecht, S. Albrecht, M. Antonello, S. Bein, L. Benato, M. Bonanomi, P. Connor, M. Eich, K. El Morabit, Y. Fischer, A. Fröhlich, C. Garbers, E. Garutti, A. Grohsjean, M. Hajheidari, J. Haller, H. R. Jabusch, G. Kasieczka, P. Keicher, R. Klanner, W. Korcari, T. Kramer, V. Kutzner, F. Labe, J. Lange, A. Lobanov, C. Matthies, A. Mehta, L. Moureaux, M. Mrowietz, A. Nigamova, Y. Nissan, A. Paasch, K. J. Pena Rodriguez, T. Quadfasel, B. Raciti, M. Rieger, D. Savoiu, J. Schindler, P. Schleper, M. Schröder, J. Schwandt, M. Sommerhalder, H. Stadie, G. Steinbrück, A. Tews, M. Wolf

Karlsruher Institut fuer Technologie, Karlsruhe, Germany
S. Brommer, M. Burkart, E. Butz, T. Chwalek, A. Dierlamm, A. Droll, N. Faltermann, M. Giffels, A. Gottmann, F. Hartmann[34], R. Hofsaess, M. Horzela, U. Husemann, J. Kieseler, M. Klute, R. Koppenhöfer, J. M. Lawhorn, M. Link, A. Lintuluoto, S. Maier, S. Mitra, M. Mormile, Th. Müller, M. Neukum, M. Oh, M. Presilla, G. Quast, K. Rabbertz, B. Regnery, N. Shadskiy, I. Shvetsov, H. J. Simonis, M. Toms[35], N. Trevisani, R. Ulrich, R. F. Von Cube, M. Wassmer, S. Wieland, F. Wittig, R. Wolf, X. Zuo

Institute of Nuclear and Particle Physics (INPP), NCSR Demokritos, Aghia Paraskevi, Greece
G. Anagnostou, G. Daskalakis, A. Kyriakis, A. Papadopoulos[34], A. Stakia

National and Kapodistrian University of Athens, Athens, Greece
P. Kontaxakis, G. Melachroinos, A. Panagiotou, I. Papavergou, I. Paraskevas, N. Saoulidou, K. Theofilatos, E. Tziaferi, K. Vellidis, I. Zisopoulos

National Technical University of Athens, Athens, Greece
G. Bakas, T. Chatzistavrou, G. Karapostoli, K. Kousouris, I. Papakrivopoulos, E. Siamarkou, G. Tsipolitis, A. Zacharopoulou

University of Ioánnina, Ioannina, Greece
K. Adamidis, I. Bestintzanos, I. Evangelou, C. Foudas, P. Gianneios, C. Kamtsikis, P. Katsoulis, P. Kokkas, P. G. Kosmoglou Kioseoglou, N. Manthos, I. Papadopoulos, J. Strologas

HUN-REN Wigner Research Centre for Physics, Budapest, Hungary
M. Bartók[36], C. Hajdu, D. Horvath[37,38], F. Sikler, V. Veszpremi

MTA-ELTE Lendület CMS Particle and Nuclear Physics Group, Eötvös Loránd University, Budapest, Hungary
M. Csanád, K. Farkas, M. M. A. Gadallah[39], Á. Kadlecsik, P. Major, K. Mandal, G. Pásztor, A. J. Rádl[40], G. I. Veres

Faculty of Informatics, University of Debrecen, Debrecen, Hungary
P. Raics, B. Ujvari, G. Zilizi

Institute of Nuclear Research ATOMKI, Debrecen, Hungary
G. Bencze, S. Czellar, J. Molnar, Z. Szillasi

Karoly Robert Campus, MATE Institute of Technology, Gyongyos, Hungary
T. Csorgo[40], F. Nemes[40], T. Novak

Panjab University, Chandigarh, India
J. Babbar, S. Bansal, S. B. Beri, V. Bhatnagar, G. Chaudhary, S. Chauhan, N. Dhingra[41], A. Kaur, A. Kaur, H. Kaur, M. Kaur, S. Kumar, K. Sandeep, T. Sheokand, J. B. Singh, A. Singla

University of Delhi, Delhi, India
A. Ahmed, A. Bhardwaj, A. Chhetri, B. C. Choudhary, A. Kumar, A. Kumar, M. Naimuddin, K. Ranjan, S. Saumya

Saha Institute of Nuclear Physics, HBNI, Kolkata, India
S. Baradia, S. Barman[42], S. Bhattacharya, S. Dutta, S. Dutta, P. Palit, S. Sarkar

Indian Institute of Technology Madras, Madras, India
M. M. Ameen, P. K. Behera, S. C. Behera, S. Chatterjee, P. Jana, P. Kalbhor, J. R. Komaragiri[43], D. Kumar[43], L. Panwar[43], P. R. Pujahari, N. R. Saha, A. Sharma, A. K. Sikdar, S. Verma

Tata Institute of Fundamental Research-A, Mumbai, India
S. Dugad, M. Kumar, G. B. Mohanty, P. Suryadevara

Tata Institute of Fundamental Research-B, Mumbai, India
A. Bala, S. Banerjee, R. M. Chatterjee, R. K. Dewanjee[44], M. Guchait, Sh. Jain, S. Karmakar, S. Kumar, G. Majumder, K. Mazumdar, S. Parolia, A. Thachayath

National Institute of Science Education and Research, An OCC of Homi Bhabha National Institute, Bhubaneswar, Odisha, India
S. Bahinipati[45], C. Kar, D. Maity[46], P. Mal, T. Mishra, V. K. Muraleedharan Nair Bindhu[46], K. Naskar[46], A. Nayak[46], P. Sadangi, P. Saha, S. K. Swain, S. Varghese[46], D. Vats[46]

Indian Institute of Science Education and Research (IISER), Pune, India
S. Acharya[47], A. Alpana, S. Dube, B. Gomber[47], B. Kansal, A. Laha, B. Sahu[47], S. Sharma

Isfahan University of Technology, Isfahan, Iran
H. Bakhshiansohi[48], E. Khazaie[49], M. Zeinali[50]

Institute for Research in Fundamental Sciences (IPM), Tehran, Iran
S. Chenarani[51], S. M. Etesami, M. Khakzad, M. Mohammadi Najafabadi

University College Dublin, Dublin, Ireland
M. Grunewald

INFN Sezione di Bari[a], Università di Bari[b], Politecnico di Bari[c], Bari, Italy
M. Abbrescia[a,b], R. Aly[a,c,18], A. Colaleo[a,b], D. Creanza[a,c], B. D'Anzi[a,b], N. De Filippis[a,c], M. De Palma[a,b], A. Di Florio[a,c], W. Elmetenawee[a,b,18], L. Fiore[a], G. Iaselli[a,c], M. Louka[a,b], G. Maggi[a,c], M. Maggi[a], I. Margjeka[a,b], V. Mastrapasqua[a,b], S. My[a,b], S. Nuzzo[a,b], A. Pellecchia[a,b], A. Pompili[a,b], G. Pugliese[a,c], R. Radogna[a], G. Ramirez-Sanchez[a,c], D. Ramos[a], A. Ranieri[a], L. Silvestris[a], F. M. Simone[a,b], Ü. Sözbilir[a], A. Stamerra[a], R. Venditti[a], P. Verwilligen[a], A. Zaza[a,b]

INFN Sezione di Bologna[a], Università di Bologna[b], Bologna, Italy
G. Abbiendi[a], C. Battilana[a,b], D. Bonacorsi[a,b], L. Borgonovi[a], R. Campanini[a,b], P. Capiluppi[a,b], A. Castro[a,b], F. R. Cavallo[a], M. Cuffiani[a,b], G. M. Dallavalle[a], T. Diotalevi[a,b], F. Fabbri[a], A. Fanfani[a,b], D. Fasanella[a,b], P. Giacomelli[a], L. Giommi[a,b], C. Grandi[a], L. Guiducci[a,b], S. Lo Meo[a,52], L. Lunerti[a,b], S. Marcellini[a], G. Masetti[a], F. L. Navarria[a,b], A. Perrotta[a], F. Primavera[a,b], A. M. Rossi[a,b], T. Rovelli[a,b]

INFN Sezione di Catania[a], Università di Catania[b], Catania, Italy
S. Costa[a,b,53], A. Di Mattia[a], R. Potenza[a,b], A. Tricomi[a,b,53], C. Tuve[a,b]

INFN Sezione di Firenze[a], Università di Firenze[b], Firenze, Italy
P. Assiouras[a], G. Barbagli[a], G. Bardelli[a,b], B. Camaiani[a,b], A. Cassese[a], R. Ceccarelli[a], V. Ciulli[a,b], C. Civinini[a], R. D'Alessandro[a,b], E. Focardi[a,b], T. Kello[a], G. Latino[a,b], P. Lenzi[a,b], M. Lizzo[a], M. Meschini[a], S. Paoletti[a], A. Papanastassiou[a,b], G. Sguazzoni[a], L. Viliani[a]

INFN Laboratori Nazionali di Frascati, Frascati, Italy
L. Benussi, S. Bianco, S. Meola[54], D. Piccolo

INFN Sezione di Genova[a], Università di Genova[b], Genoa, Italy
P. Chatagnon[a], F. Ferro[a], E. Robutti[a], S. Tosi[a,b]

INFN Sezione di Milano-Bicocca[a], Università di Milano-Bicocca[b], Milan, Italy
A. Benaglia[a], G. Boldrini[a,b], F. Brivio[a], F. Cetorelli[a], F. De Guio[a,b], M. E. Dinardo[a,b], P. Dini[a], S. Gennai[a], R. Gerosa[a,b], A. Ghezzi[a,b], P. Govoni[a,b], L. Guzzi[a], M. T. Lucchini[a,b], M. Malberti[a], S. Malvezzi[a], A. Massironi[a], D. Menasce[a], L. Moroni[a], M. Paganoni[a,b], D. Pedrini[a], B. S. Pinolini[a], S. Ragazzi[a,b], T. Tabarelli de Fatis[a,b], D. Zuolo[a]

INFN Sezione di Napoli[a], Università di Napoli 'Federico II'[b], Napoli, Italy; Università della Basilicata[c], Potenza, Italy; Scuola Superiore Meridionale (SSM)[d], Naples, Italy
S. Buontempo[a], A. Cagnotta[a,b], F. Carnevali[a,b], N. Cavallo[a,c], A. De Iorio[a,b], F. Fabozzi[a,c], A. O. M. Iorio[a,b], L. Lista[a,b,55], P. Paolucci[a,34], B. Rossi[a], C. Sciacca[a,b]

INFN Sezione di Padova[a], Università di Padova[b], Padova, Italy; Università di Trento[c], Trento, Italy
R. Ardino[a], P. Azzi[a], N. Bacchetta[a,56], M. Bellato[a], D. Bisello[a,b], P. Bortignon[a], A. Bragagnolo[a,b], R. Carlin[a,b], P. Checchia[a], T. Dorigo[a], F. Gasparini[a,b], U. Gasparini[a,b], E. Lusiani[a], M. Margoni[a,b], F. Marini[a], M. Migliorini[a,b], J. Pazzini[a,b], P. Ronchese[a,b], R. Rossin[a,b], F. Simonetto[a,b], G. Strong[a], M. Tosi[a,b], A. Triossi[a,b], S. Ventura[a], H. Yarar[a,b], M. Zanetti[a,b], P. Zotto[a,b], A. Zucchetta[a,b], G. Zumerle[a,b]

INFN Sezione di Pavia[a], Università di Pavia[b], Pavia, Italy
S. Abu Zeid[a,21], C. Aimè[a,b], A. Braghieri[a], S. Calzaferri[a], D. Fiorina[a], P. Montagna[a,b], V. Re[a], C. Riccardi[a,b], P. Salvini[a], I. Vai[a,b], P. Vitulo[a,b]

INFN Sezione di Perugia[a], Università di Perugia[b], Perugia, Italy
S. Ajmal[a,b], P. Asenov[a,57], G. M. Bilei[a], D. Ciangottini[a,b], L. Fanò[a,b], M. Magherini[a,b], G. Mantovani[a,b], V. Mariani[a,b], M. Menichelli[a], F. Moscatelli[a,57], A. Rossi[a,b], A. Santocchia[a,b], D. Spiga[a], T. Tedeschi[a,b]

INFN Sezione di Pisa[a], Università di Pisa[b], Scuola Normale Superiore di Pisa[c], Pisa, Italy; Università di Siena[d], Siena, Italy
P. Azzurri[a], G. Bagliesi[a], R. Bhattacharya[a], L. Bianchini[a,b], T. Boccali[a], E. Bossini[a], D. Bruschini[a,c], R. Castaldi[a], M. A. Ciocci[a,b], M. Cipriani[a,b], V. D'Amante[a,d], R. Dell'Orso[a], S. Donato[a], A. Giassi[a], F. Ligabue[a,c], D. Matos Figueiredo[a], A. Messineo[a,b], M. Musich[a,b], F. Palla[a], A. Rizzi[a,b], G. Rolandi[a,c], S. Roy Chowdhury[a], T. Sarkar[a], A. Scribano[a], P. Spagnolo[a], R. Tenchini[a], G. Tonelli[a,b], N. Turini[a,d], A. Venturi[a], P. G. Verdini[a]

INFN Sezione di Roma[a], Sapienza Università di Roma[b], Rome, Italy
P. Barria[a], M. Campana[a,b], F. Cavallari[a], L. Cunqueiro Mendez[a,b], D. Del Re[a,b], E. Di Marco[a], M. Diemoz[a], F. Errico[a,b], E. Longo[a,b], P. Meridiani[a], J. Mijuskovic[a,b], G. Organtini[a,b], F. Pandolfi[a], R. Paramatti[a,b], C. Quaranta[a,b], S. Rahatlou[a,b], C. Rovelli[a], F. Santanastasio[a,b], L. Soffi[a]

INFN Sezione di Torino[a], Università di Torino[b], Torino, Italy; Università del Piemonte Orientale[c], Novara, Italy
N. Amapane[a,b], R. Arcidiacono[a,c], S. Argiro[a,b], M. Arneodo[a,c], N. Bartosik[a], R. Bellan[a,b], A. Bellora[a,b], C. Biino[a], N. Cartiglia[a], M. Costa[a,b], R. Covarelli[a,b], N. Demaria[a], L. Finco[a], M. Grippo[a,b], B. Kiani[a,b], F. Legger[a], F. Luongo[a,b], C. Mariotti[a], S. Maselli[a], A. Mecca[a,b], E. Migliore[a,b], M. Monteno[a], R. Mulargia[a], M. M. Obertino[a,b], G. Ortona[a], L. Pacher[a,b], N. Pastrone[a], M. Pelliccioni[a], M. Ruspa[a,c], F. Siviero[a,b], V. Sola[a,b], A. Solano[a,b], A. Staiano[a], C. Tarricone[a,b], D. Trocino[a], G. Umoret[a,b], E. Vlasov[a,b]

INFN Sezione di Trieste[a], Università di Trieste[b], Trieste, Italy
S. Belforte[a], V. Candelise[a,b], M. Casarsa[a], F. Cossutti[a], K. De Leo[a,b], G. Della Ricca[a,b]

Kyungpook National University, Daegu, Korea
S. Dogra, J. Hong, C. Huh, B. Kim, D. H. Kim, J. Kim, H. Lee, S. W. Lee, C. S. Moon, Y. D. Oh, M. S. Ryu, S. Sekmen, Y. C. Yang

Department of Mathematics and Physics-GWNU, Gangneung, Korea
M. S. Kim

Chonnam National University, Institute for Universe and Elementary Particles, Kwangju, Korea
G. Bak, P. Gwak, H. Kim, D. H. Moon

Hanyang University, Seoul, Korea
E. Asilar, D. Kim, T. J. Kim, J. A. Merlin

Korea University, Seoul, Korea
S. Choi, S. Han, B. Hong, K. Lee, K. S. Lee, S. Lee, J. Park, S. K. Park, J. Yoo

Department of Physics, Kyung Hee University, Seoul, Korea
J. Goh, S. Yang

Sejong University, Seoul, Korea
H. S. Kim, Y. Kim, S. Lee

Seoul National University, Seoul, Korea
J. Almond, J. H. Bhyun, J. Choi, W. Jun, J. Kim, S. Ko, H. Kwon, H. Lee, J. Lee, J. Lee, B. H. Oh, S. B. Oh, H. Seo, U. K. Yang, I. Yoon

University of Seoul, Seoul, Korea
W. Jang, D. Y. Kang, Y. Kang, S. Kim, B. Ko, J. S. H. Lee, Y. Lee, I. C. Park, Y. Roh, I. J. Watson

Yonsei University, Department of Physics, Seoul, Korea
S. Ha, H. D. Yoo

Sungkyunkwan University, Suwon, Korea
M. Choi, M. R. Kim, H. Lee, Y. Lee, I. Yu

College of Engineering and Technology, American University of the Middle East (AUM), Dasman, Kuwait
T. Beyrouthy, Y. Maghrbi

Riga Technical University, Riga, Latvia
K. Dreimanis, A. Gaile, G. Pikurs, A. Potrebko, M. Seidel, V. Veckalns[58]

University of Latvia (LU), Riga, Latvia
N. R. Strautnieks

Vilnius University, Vilnius, Lithuania
M. Ambrozas, A. Juodagalvis, A. Rinkevicius, G. Tamulaitis

National Centre for Particle Physics, Universiti Malaya, Kuala Lumpur, Malaysia
N. Bin Norjoharuddeen, I. Yusuff[59], Z. Zolkapli

Universidad de Sonora (UNISON), Hermosillo, Mexico
J. F. Benitez, A. Castaneda Hernandez, H. A. Encinas Acosta, L. G. Gallegos Maríñez, M. León Coello, J. A. Murillo Quijada, A. Sehrawat, L. Valencia Palomo

Centro de Investigacion y de Estudios Avanzados del IPN, Mexico City, Mexico
G. Ayala, H. Castilla-Valdez, E. De La Cruz-Burelo, I. Heredia-De La Cruz[60], R. Lopez-Fernandez, C. A. Mondragon Herrera, A. Sánchez Hernández

Universidad Iberoamericana, Mexico City, Mexico
C. Oropeza Barrera, M. Ramírez García

Benemerita Universidad Autonoma de Puebla, Puebla, Mexico
I. Bautista, I. Pedraza, H. A. Salazar Ibarguen, C. Uribe Estrada

University of Montenegro, Podgorica, Montenegro
I. Bubanja, N. Raicevic

University of Canterbury, Christchurch, New Zealand
P. H. Butler

National Centre for Physics, Quaid-I-Azam University, Islamabad, Pakistan
A. Ahmad, M. I. Asghar, A. Awais, M. I. M. Awan, H. R. Hoorani, W. A. Khan

Faculty of Computer Science, Electronics and Telecommunications, AGH University of Krakow, Kraków, Poland
V. Avati, L. Grzanka, M. Malawski

National Centre for Nuclear Research, Swierk, Poland
H. Bialkowska, M. Bluj, B. Boimska, M. Górski, M. Kazana, M. Szleper, P. Zalewski

Institute of Experimental Physics, Faculty of Physics, University of Warsaw, Warsaw, Poland
K. Bunkowski, K. Doroba, A. Kalinowski, M. Konecki, J. Krolikowski, A. Muhammad

Warsaw University of Technology, Warsaw, Poland
K. Pozniak, W. Zabolotny

Laboratório de Instrumentação e Física Experimental de Partículas, Lisbon, Portugal
M. Araujo, D. Bastos, C. Beirão Da Cruz E Silva, A. Boletti, M. Bozzo, T. Camporesi, G. Da Molin, P. Faccioli, M. Gallinaro, J. Hollar, N. Leonardo, T. Niknejad, A. Petrilli, M. Pisano, J. Seixas, J. Varela, J. W. Wulff

Faculty of Physics, University of Belgrade, Belgrade, Serbia
P. Adzic, P. Milenovic

VINCA Institute of Nuclear Sciences, University of Belgrade, Belgrade, Serbia
M. Dordevic, J. Milosevic, V. Rekovic

Centro de Investigaciones Energéticas Medioambientales y Tecnológicas (CIEMAT), Madrid, Spain
M. Aguilar-Benitez, J. Alcaraz Maestre, Cristina F. Bedoya, M. Cepeda, M. Cerrada, N. Colino, B. De La Cruz, A. Delgado Peris, A. Escalante Del Valle, D. Fernández Del Val, J. P. Fernández Ramos, J. Flix, M. C. Fouz, O. Gonzalez Lopez, S. Goy Lopez, J. M. Hernandez, M. I. Josa, D. Moran, C. M. Morcillo Perez, Á. Navarro Tobar, C. Perez Dengra, A. Pérez-Calero Yzquierdo, J. Puerta Pelayo, I. Redondo, D. D. Redondo Ferrero, L. Romero, S. Sánchez Navas, L. Urda Gómez, J. Vazquez Escobar, C. Willmott

Universidad Autónoma de Madrid, Madrid, Spain
J. F. de Trocóniz

Universidad de Oviedo, Instituto Universitario de Ciencias y Tecnologías Espaciales de Asturias (ICTEA), Oviedo, Spain
B. Alvarez Gonzalez, J. Cuevas, J. Fernandez Menendez, S. Folgueras, I. Gonzalez Caballero, J. R. González Fernández, E. Palencia Cortezon, C. Ramón Álvarez, V. Rodríguez Bouza, A. Soto Rodríguez, A. Trapote, C. Vico Villalba, P. Vischia

Instituto de Física de Cantabria (IFCA), CSIC-Universidad de Cantabria, Santander, Spain
S. Bhowmik, S. Blanco Fernández, J. A. Brochero Cifuentes, I. J. Cabrillo, A. Calderon, J. Duarte Campderros, M. Fernandez, G. Gomez, C. Lasaosa García, C. Martinez Rivero, P. Martinez Ruiz del Arbol, F. Matorras, P. Matorras Cuevas, E. Navarrete Ramos, J. Piedra Gomez, L. Scodellaro, I. Vila, J. M. Vizan Garcia

University of Colombo, Colombo, Sri Lanka
M. K. Jayananda, B. Kailasapathy[61], D. U. J. Sonnadara, D. D. C. Wickramarathna

Department of Physics, University of Ruhuna, Matara, Sri Lanka
W. G. D. Dharmaratna[62], K. Liyanage, N. Perera, N. Wickramage

CERN, European Organization for Nuclear Research, Geneva, Switzerland
D. Abbaneo, C. Amendola, E. Auffray, G. Auzinger, J. Baechler, D. Barney, A. Bermúdez Martínez, M. Bianco, B. Bilin, A. A. Bin Anuar, A. Bocci, C. Botta, E. Brondolin, C. Caillol, G. Cerminara, N. Chernyavskaya, D. d'Enterria, A. Dabrowski, A. David, A. De Roeck, M. M. Defranchis, M. Deile, M. Dobson, L. Forthomme, G. Franzoni, W. Funk, S. Giani, D. Gigi, K. Gill, F. Glege, L. Gouskos, M. Haranko, J. Hegeman, B. Huber, V. Innocente, T. James, P. Janot, S. Laurila, P. Lecoq, E. Leutgeb, C. Lourenço, B. Maier, L. Malgeri, M. Mannelli, A. C. Marini, M. Matthewman, F. Meijers, S. Mersi, E. Meschi, V. Milosevic, F. Monti, F. Moortgat, M. Mulders, I. Neutelings, S. Orfanelli, F. Pantaleo, G. Petrucciani, A. Pfeiffer, M. Pierini, D. Piparo, H. Qu, D. Rabady, G. Reales Gutiérrez, M. Rovere, H. Sakulin, S. Scarfi, C. Schwick, M. Selvaggi, A. Sharma, K. Shchelina, P. Silva, P. Sphicas[63], A. G. Stahl Leiton, A. Steen, S. Summers, D. Treille, P. Tropea, A. Tsirou, D. Walter, J. Wanczyk[64], J. Wang, S. Wuchterl, P. Zehetner, P. Zejdl, W. D. Zeuner

Paul Scherrer Institut, Villigen, Switzerland
T. Bevilacqua[65], L. Caminada[65], A. Ebrahimi, W. Erdmann, R. Horisberger, Q. Ingram, H. C. Kaestli, D. Kotlinski, C. Lange, M. Missiroli[65], L. Noehte[65], T. Rohe

ETH Zurich-Institute for Particle Physics and Astrophysics (IPA), Zurich, Switzerland
T. K. Aarrestad, K. Androsov[64], M. Backhaus, A. Calandri, C. Cazzaniga, K. Datta, A. De Cosa, G. Dissertori, M. Dittmar, M. Donegà, F. Eble, M. Galli, K. Gedia, F. Glessgen, C. Grab, D. Hits, W. Lustermann, A.-M. Lyon, R. A. Manzoni, M. Marchegiani, L. Marchese, C. Martin Perez, A. Mascellani[64], F. Nessi-Tedaldi, F. Pauss, V. Perovic, S. Pigazzini, C. Reissel, T. Reitenspiess, B. Ristic, F. Riti, D. Ruini, R. Seidita, J. Steggemann[64], D. Valsecchi, R. Wallny

Universität Zürich, Zurich, Switzerland
C. Amsler[66], P. Bärtschi, D. Brzhechko, M. F. Canelli, K. Cormier, J. K. Heikkilä, M. Huwiler, W. Jin, A. Jofrehei, B. Kilminster, S. Leontsinis, S. P. Liechti, A. Macchiolo, P. Meiring, U. Molinatti, A. Reimers, P. Robmann, S. Sanchez Cruz, M. Senger, Y. Takahashi, R. Tramontano

National Central University, Chung-Li, Taiwan
C. Adloff[67], D. Bhowmik, C. M. Kuo, W. Lin, P. K. Rout, P. C. Tiwari[43], S. S. Yu

National Taiwan University (NTU), Taipei, Taiwan
L. Ceard, Y. Chao, K. F. Chen, P. s. Chen, Z. g. Chen, W. -S. Hou, T. h. Hsu, Y. w. Kao, R. Khurana, G. Kole, Y. y. Li, R.-S. Lu, E. Paganis, X. f. Su, J. Thomas-Wilsker, L. s. Tsai, H. y. Wu, E. Yazgan

High Energy Physics Research Unit, Department of Physics, Faculty of Science, Chulalongkorn University, Bangkok, Thailand
C. Asawatangtrakuldee, N. Srimanobhas, V. Wachirapusitanand

Çukurova University, Physics Department, Science and Art Faculty, Adana, Turkey
D. Agyel, F. Boran, Z. S. Demiroglu, F. Dolek, I. Dumanoglu[68], E. Eskut, Y. Guler[69], E. Gurpinar Guler[69], C. Isik, O. Kara, A. Kayis Topaksu, U. Kiminsu, G. Onengut, K. Ozdemir[70], A. Polatoz, B. Tali[71], U. G. Tok, S. Turkcapar, E. Uslan, I. S. Zorbakir

Physics Department, Middle East Technical University, Ankara, Turkey
M. Yalvac[72]

Bogazici University, Istanbul, Turkey
B. Akgun, I. O. Atakisi, E. Gülmez, M. Kaya[73], O. Kaya[74], S. Tekten[75]

Istanbul Technical University, Istanbul, Turkey
A. Cakir, K. Cankocak[68,76], Y. Komurcu, S. Sen[77]

Istanbul University, Istanbul, Turkey
O. Aydilek, S. Cerci[71], V. Epshteyn, B. Hacisahinoglu, I. Hos[78], B. Kaynak, S. Ozkorucuklu, O. Potok, H. Sert, C. Simsek, C. Zorbilmez

Yildiz Technical University, Istanbul, Turkey
B. Isildak[79], D. Sunar Cerci[71]

Institute for Scintillation Materials of National Academy of Science of Ukraine, Kharkiv, Ukraine
A. Boyaryntsev, B. Grynyov

Kharkiv Institute of Physics and Technology, National Science Centre, Kharkiv, Ukraine
L. Levchuk

University of Bristol, Bristol, UK
D. Anthony, J. J. Brooke, A. Bundock, F. Bury, E. Clement, D. Cussans, H. Flacher, M. Glowacki, J. Goldstein, H. F. Heath, L. Kreczko, S. Paramesvaran, S. Seif El Nasr-Storey, V. J. Smith, N. Stylianou[80], K. Walkingshaw Pass, R. White

Rutherford Appleton Laboratory, Didcot, UK
A. H. Ball, K. W. Bell, A. Belyaev[81], C. Brew, R. M. Brown, D. J. A. Cockerill, C. Cooke, K. V. Ellis, K. Harder, S. Harper, M.-L. Holmberg[82], J. Linacre, K. Manolopoulos, D. M. Newbold, E. Olaiya, D. Petyt, T. Reis, G. Salvi, T. Schuh, C. H. Shepherd-Themistocleous, I. R. Tomalin, T. Williams

Imperial College, London, UK
R. Bainbridge, P. Bloch, C. E. Brown, O. Buchmuller, V. Cacchio, C. A. Carrillo Montoya, G. S. Chahal[83], D. Colling, J. S. Dancu, I. Das, P. Dauncey, G. Davies, J. Davies, M. Della Negra, S. Fayer, G. Fedi, G. Hall, M. H. Hassanshahi, A. Howard, G. Iles, M. Knight, J. Langford, J. León Holgado, L. Lyons, A.-M. Magnan, S. Malik, M. Mieskolainen, J. Nash[84], M. Pesaresi, B. C. Radburn-Smith, A. Richards, A. Rose, C. Seez, R. Shukla, A. Tapper, K. Uchida, G. P. Uttley, L. H. Vage, T. Virdee[34], M. Vojinovic, N. Wardle, D. Winterbottom

Brunel University, Uxbridge, UK
K. Coldham, J. E. Cole, A. Khan, P. Kyberd, I. D. Reid

Baylor University, Waco, TX, USA
S. Abdullin, A. Brinkerhoff, B. Caraway, J. Dittmann, K. Hatakeyama, J. Hiltbrand, B. McMaster, M. Saunders, S. Sawant, C. Sutantawibul, J. Wilson

Catholic University of America, Washington, DC, USA
R. Bartek, A. Dominguez, C. Huerta Escamilla, A. E. Simsek, R. Uniyal, A. M. Vargas Hernandez

The University of Alabama, Tuscaloosa, AL, USA
B. Bam, R. Chudasama, S. I. Cooper, S. V. Gleyzer, C. U. Perez, P. Rumerio[85], E. Usai, R. Yi

Boston University, Boston, MA, USA
A. Akpinar, D. Arcaro, C. Cosby, Z. Demiragli, C. Erice, C. Fangmeier, C. Fernandez Madrazo, E. Fontanesi, D. Gastler, F. Golf, S. Jeon, I. Reed, J. Rohlf, K. Salyer, D. Sperka, D. Spitzbart, I. Suarez, A. Tsatsos, S. Yuan, A. G. Zecchinelli

Brown University, Providence, RI, USA
G. Benelli, X. Coubez[29], D. Cutts, M. Hadley, U. Heintz, J. M. Hogan[86], T. Kwon, G. Landsberg, K. T. Lau, D. Li, J. Luo, S. Mondal, M. Narain[†], N. Pervan, S. Sagir[87], F. Simpson, M. Stamenkovic, W. Y. Wong, X. Yan, W. Zhang

University of California, Davis, Davis, CA, USA
S. Abbott, J. Bonilla, C. Brainerd, R. Breedon, M. Calderon De La Barca Sanchez, M. Chertok, M. Citron, J. Conway, P. T. Cox, R. Erbacher, F. Jensen, O. Kukral, G. Mocellin, M. Mulhearn, D. Pellett, W. Wei, Y. Yao, F. Zhang

University of California, Los Angeles, CA, USA
M. Bachtis, R. Cousins, A. Datta, G. Flores Avila, J. Hauser, M. Ignatenko, M. A. Iqbal, T. Lam, E. Manca, A. Nunez Del Prado, D. Saltzberg, V. Valuev

University of California, Riverside, Riverside, CA, USA
R. Clare, J. W. Gary, M. Gordon, G. Hanson, W. Si, S. Wimpenny †

University of California, San Diego, La Jolla, CA, USA
J. G. Branson, S. Cittolin, S. Cooperstein, D. Diaz, J. Duarte, L. Giannini, J. Guiang, R. Kansal, V. Krutelyov, R. Lee, J. Letts, M. Masciovecchio, F. Mokhtar, S. Mukherjee, M. Pieri, M. Quinnan, B. V. Sathia Narayanan, V. Sharma, M. Tadel, E. Vourliotis, F. Würthwein, Y. Xiang, A. Yagil

Department of Physics, University of California, Santa Barbara, Santa Barbara, CA, USA
A. Barzdukas, L. Brennan, C. Campagnari, A. Dorsett, J. Incandela, J. Kim, A. J. Li, P. Masterson, H. Mei, J. Richman, U. Sarica, R. Schmitz, F. Setti, J. Sheplock, D. Stuart, T. Á. Vámi, S. Wang

California Institute of Technology, Pasadena, CA, USA
A. Bornheim, O. Cerri, A. Latorre, J. Mao, H. B. Newman, M. Spiropulu, J. R. Vlimant, C. Wang, S. Xie, R. Y. Zhu

Carnegie Mellon University, Pittsburgh, PA, USA
J. Alison, S. An, M. B. Andrews, P. Bryant, M. Cremonesi, V. Dutta, T. Ferguson, A. Harilal, C. Liu, T. Mudholkar, S. Murthy, M. Paulini, A. Roberts, A. Sanchez, W. Terrill

University of Colorado Boulder, Boulder, CO, USA
J. P. Cumalat, W.T. Ford, A. Hassani, G. Karathanasis, E. MacDonald, N. Manganelli, A. Perloff, C. Savard, N. Schonbeck, K. Stenson, K. A. Ulmer, S. R. Wagner, N. Zipper

Cornell University, Ithaca, NY, USA
J. Alexander, S. Bright-Thonney, X. Chen, D. J. Cranshaw, J. Fan, X. Fan, D. Gadkari, S. Hogan, P. Kotamnives, J. Monroy, M. Oshiro, J. R. Patterson, J. Reichert, M. Reid, A. Ryd, J. Thom, P. Wittich, R. Zou

Fermi National Accelerator Laboratory, Batavia, IL, USA
M. Albrow, M. Alyari, O. Amram, G. Apollinari, A. Apresyan, L. A. T. Bauerdick, D. Berry, J. Berryhill, P. C. Bhat, K. Burkett, J. N. Butler, A. Canepa, G. B. Cerati, H. W. K. Cheung, F. Chlebana, G. Cummings, J. Dickinson, I. Dutta, V. D. Elvira, Y. Feng, J. Freeman, A. Gandrakota, Z. Gecse, L. Gray, D. Green, A. Grummer, S. Grünendahl, D. Guerrero, O. Gutsche, R. M. Harris, R. Heller, T. C. Herwig, J. Hirschauer, L. Horyn, B. Jayatilaka, S. Jindariani, M. Johnson, U. Joshi, T. Klijnsma, B. Klima, K. H. M. Kwok, S. Lammel, D. Lincoln, R. Lipton, T. Liu, C. Madrid, K. Maeshima, C. Mantilla, D. Mason, P. McBride, P. Merkel, S. Mrenna, S. Nahn, J. Ngadiuba, D. Noonan, V. Papadimitriou, N. Pastika, K. Pedro, C. Pena [88], F. Ravera, A. Reinsvold Hall [89], L. Ristori, E. Sexton-Kennedy, N. Smith, A. Soha, L. Spiegel, S. Stoynev, J. Strait, L. Taylor, S. Tkaczyk, N. V. Tran, L. Uplegger, E. W. Vaandering, I. Zoi

University of Florida, Gainesville, FL, USA
C. Aruta, P. Avery, D. Bourilkov, L. Cadamuro, P. Chang, V. Cherepanov, R. D. Field, E. Koenig, M. Kolosova, J. Konigsberg, A. Korytov, K. H. Lo, K. Matchev, N. Menendez, G. Mitselmakher, K. Mohrman, A. Muthirakalayil Madhu, N. Rawal, D. Rosenzweig, S. Rosenzweig, K. Shi, J. Wang

Florida State University, Tallahassee, FL, USA
T. Adams, A. Al Kadhim, A. Askew, N. Bower, R. Habibullah, V. Hagopian, R. Hashmi, R. S. Kim, S. Kim, T. Kolberg, G. Martinez, H. Prosper, P. R. Prova, M. Wulansatiti, R. Yohay, J. Zhang

Florida Institute of Technology, Melbourne, FL, USA
B. Alsufyani, M. M. Baarmand, S. Butalla, T. Elkafrawy [21], M. Hohlmann, R. Kumar Verma, M. Rahmani, E. Yanes

University of Illinois Chicago, Chicago, USA
M. R. Adams, A. Baty, C. Bennett, R. Cavanaugh, R. Escobar Franco, O. Evdokimov, C. E. Gerber, D. J. Hofman, J. h. Lee, D. S. Lemos, A. H. Merrit, C. Mills, S. Nanda, G. Oh, B. Ozek, D. Pilipovic, R. Pradhan, T. Roy, S. Rudrabhatla, M. B. Tonjes, N. Varelas, Z. Ye, J. Yoo

The University of Iowa, Iowa City, IA, USA
M. Alhusseini, D. Blend, K. Dilsiz[90], L. Emediato, G. Karaman, O. K. Köseyan, J.-P. Merlo, A. Mestvirishvili[91], J. Nachtman, O. Neogi, H. Ogul[92], Y. Onel, A. Penzo, C. Snyder, E. Tiras[93]

Johns Hopkins University, Baltimore, MD, USA
B. Blumenfeld, L. Corcodilos, J. Davis, A. V. Gritsan, L. Kang, S. Kyriacou, P. Maksimovic, M. Roguljic, J. Roskes, S. Sekhar, M. Swartz

The University of Kansas, Lawrence, KS, USA
A. Abreu, L. F. Alcerro Alcerro, J. Anguiano, P. Baringer, A. Bean, Z. Flowers, D. Grove, J. King, G. Krintiras, M. Lazarovits, C. Le Mahieu, C. Lindsey, J. Marquez, N. Minafra, M. Murray, M. Nickel, M. Pitt, S. Popescu[94], C. Rogan, C. Royon, R. Salvatico, S. Sanders, C. Smith, Q. Wang, G. Wilson

Kansas State University, Manhattan, KS, USA
B. Allmond, A. Ivanov, K. Kaadze, A. Kalogeropoulos, D. Kim, Y. Maravin, K. Nam, J. Natoli, D. Roy, G. Sorrentino

Lawrence Livermore National Laboratory, Livermore, CA, USA
F. Rebassoo, D. Wright

University of Maryland, College Park, MD, USA
A. Baden, A. Belloni, Y. M. Chen, S. C. Eno, N. J. Hadley, S. Jabeen, R. G. Kellogg, T. Koeth, Y. Lai, S. Lascio, A. C. Mignerey, S. Nabili, C. Palmer, C. Papageorgakis, M. M. Paranjpe, L. Wang

Massachusetts Institute of Technology, Cambridge, MA, USA
J. Bendavid, W. Busza, I. A. Cali, M. D'Alfonso, J. Eysermans, C. Freer, G. Gomez-Ceballos, M. Goncharov, G. Grosso, P. Harris, D. Hoang, D. Kovalskyi, J. Krupa, L. Lavezzo, Y.-J. Lee, K. Long, C. Mironov, C. Paus, D. Rankin, C. Roland, G. Roland, S. Rothman, G. S. F. Stephans, Z. Wang, B. Wyslouch, T. J. Yang

University of Minnesota, Minneapolis, MN, USA
B. Crossman, B. M. Joshi, C. Kapsiak, M. Krohn, D. Mahon, J. Mans, B. Marzocchi, S. Pandey, M. Revering, R. Rusack, R. Saradhy, N. Schroeder, N. Strobbe, M. A. Wadud

University of Mississippi, Oxford, MS, USA
L. M. Cremaldi

University of Nebraska-Lincoln, Lincoln, NE, USA
K. Bloom, D. R. Claes, G. Haza, J. Hossain, C. Joo, I. Kravchenko, J. E. Siado, W. Tabb, A. Vagnerini, A. Wightman, F. Yan, D. Yu

State University of New York at Buffalo, Buffalo, NY, USA
H. Bandyopadhyay, L. Hay, I. Iashvili, A. Kharchilava, M. Morris, D. Nguyen, S. Rappoccio, H. Rejeb Sfar, A. Williams

Northeastern University, Boston, MA, USA
G. Alverson, E. Barberis, J. Dervan, Y. Haddad, Y. Han, A. Krishna, J. Li, M. Lu, G. Madigan, R. Mccarthy, D. M. Morse, V. Nguyen, T. Orimoto, A. Parker, L. Skinnari, A. Tishelman-Charny, B. Wang, D. Wood

Northwestern University, Evanston, IL, USA
S. Bhattacharya, J. Bueghly, Z. Chen, S. Dittmer, K. A. Hahn, Y. Liu, Y. Miao, D. G. Monk, M. H. Schmitt, A. Taliercio, M. Velasco

University of Notre Dame, Notre Dame, IN, USA
G. Agarwal, R. Band, R. Bucci, S. Castells, A. Das, R. Goldouzian, M. Hildreth, K. W. Ho, K. Hurtado Anampa, T. Ivanov, C. Jessop, K. Lannon, J. Lawrence, N. Loukas, L. Lutton, J. Mariano, N. Marinelli, I. Mcalister, T. McCauley, C. Mcgrady, C. Moore, Y. Musienko[17], H. Nelson, M. Osherson, A. Piccinelli, R. Ruchti, A. Townsend, Y. Wan, M. Wayne, H. Yockey, M. Zarucki, L. Zygala

The Ohio State University, Columbus, OH, USA
A. Basnet, B. Bylsma, M. Carrigan, L.S. Durkin, C. Hill, M. Joyce, M. Nunez Ornelas, K. Wei, B. L. Winer, B. R. Yates

Princeton University, Princeton, NJ, USA
F. M. Addesa, H. Bouchamaoui, P. Das, G. Dezoort, P. Elmer, A. Frankenthal, B. Greenberg, N. Haubrich, G. Kopp, S. Kwan, D. Lange, A. Loeliger, D. Marlow, I. Ojalvo, J. Olsen, A. Shevelev, D. Stickland, C. Tully

University of Puerto Rico, Mayaguez, PR, USA
S. Malik

Purdue University, West Lafayette, IN, USA
A. S. Bakshi, V. E. Barnes, S. Chandra, R. Chawla, S. Das, A. Gu, L. Gutay, M. Jones, A. W. Jung, D. Kondratyev, A. M. Koshy, M. Liu, G. Negro, N. Neumeister, G. Paspalaki, S. Piperov, V. Scheurer, J. F. Schulte, M. Stojanovic, J. Thieman, A. K. Virdi, F. Wang, W. Xie

Purdue University Northwest, Hammond, IN, USA
J. Dolen, N. Parashar, A. Pathak

Rice University, Houston, TX, USA
D. Acosta, T. Carnahan, K. M. Ecklund, P. J. Fernández Manteca, S. Freed, P. Gardner, F. J. M. Geurts, W. Li, O. Miguel Colin, B. P. Padley, R. Redjimi, J. Rotter, E. Yigitbasi, Y. Zhang

University of Rochester, Rochester, NY, USA
A. Bodek, P. de Barbaro, R. Demina, J. L. Dulemba, A. Garcia-Bellido, O. Hindrichs, A. Khukhunaishvili, N. Parmar, P. Parygin[35], E. Popova[35], R. Taus

The Rockefeller University, New York, NY, USA
K. Goulianos

Rutgers, The State University of New Jersey, Piscataway, NJ, USA
B. Chiarito, J. P. Chou, Y. Gershtein, E. Halkiadakis, A. Hart, M. Heindl, D. Jaroslawski, O. Karacheban[32], I. Laflotte, A. Lath, R. Montalvo, K. Nash, H. Routray, S. Salur, S. Schnetzer, S. Somalwar, R. Stone, S. A. Thayil, S. Thomas, J. Vora, H. Wang

University of Tennessee, Knoxville, TN, USA
H. Acharya, D. Ally, A. G. Delannoy, S. Fiorendi, S. Higginbotham, T. Holmes, A. R. Kanuganti, N. Karunarathna, L. Lee, E. Nibigira, S. Spanier

Texas A&M University, College Station, TX, USA
D. Aebi, M. Ahmad, O. Bouhali[95], R. Eusebi, J. Gilmore, T. Huang, T. Kamon[96], H. Kim, S. Luo, R. Mueller, D. Overton, D. Rathjens, A. Safonov

Texas Tech University, Lubbock, TX, USA
N. Akchurin, J. Damgov, V. Hegde, A. Hussain, Y. Kazhykarim, K. Lamichhane, S. W. Lee, A. Mankel, T. Peltola, I. Volobouev, A. Whitbeck

Vanderbilt University, Nashville, TN, USA
E. Appelt, Y. Chen, S. Greene, A. Gurrola, W. Johns, R. Kunnawalkam Elayavalli, A. Melo, F. Romeo, P. Sheldon, S. Tuo, J. Velkovska, J. Viinikainen

University of Virginia, Charlottesville, VA, USA
B. Cardwell, B. Cox, J. Hakala, R. Hirosky, A. Ledovskoy, C. Neu, C. E. Perez Lara

Wayne State University, Detroit, MI, USA
P. E. Karchin

University of Wisconsin-Madison, Madison, WI, USA
A. Aravind, S. Banerjee, K. Black, T. Bose, S. Dasu, I. De Bruyn, P. Everaerts, C. Galloni, H. He, M. Herndon, A. Herve, C. K. Koraka, A. Lanaro, R. Loveless, J. Madhusudanan Sreekala, A. Mallampalli, A. Mohammadi, S. Mondal, G. Parida, D. Pinna, A. Savin, V. Shang, V. Sharma, W. H. Smith, D. Teague, H. F. Tsoi, W. Vetens, A. Warden

Authors Affiliated with an Institute or an International Laboratory Covered by a Cooperation Agreement with CERN, Geneva, Switzerland
S. Afanasiev, V. Andreev, Yu. Andreev, T. Aushev, M. Azarkin, A. Babaev, A. Belyaev, V. Blinov[97], E. Boos, V. Borshch, D. Budkouski, M. Chadeeva[97], V. Chekhovsky, R. Chistov[97], A. Dermenev, T. Dimova[97], D. Druzhkin[98], M. Dubinin[88], L. Dudko, A. Ershov, G. Gavrilov, V. Gavrilov, S. Gninenko, V. Golovtcov, N. Golubev, I. Golutvin, I. Gorbunov, Y. Ivanov, V. Kachanov, V. Karjavine, A. Karneyeu, V. Kim[97], M. Kirakosyan, D. Kirpichnikov, M. Kirsanov, V. Klyukhin, O. Kodolova[99], V. Korenkov, A. Kozyrev[97], N. Krasnikov, A. Lanev, P. Levchenko[100], O. Lukina, N. Lychkovskaya, V. Makarenko, A. Malakhov, V. Matveev[97], V. Murzin, A. Nikitenko[99,101], S. Obraztsov, V. Oreshkin, V. Palichik, V. Perelygin, S. Petrushanko, S. Polikarpov[97], V. Popov, O. Radchenko[97], M. Savina, V. Savrin, V. Shalaev, S. Shmatov, S. Shulha, Y. Skovpen[97], S. Slabospitskii, V. Smirnov, A. Snigirev, D. Sosnov, V. Sulimov, E. Tcherniaev, A. Terkulov, O. Teryaev, I. Tlisova, A. Toropin, L. Uvarov, A. Uzunian, I. Vardanyan, A. Vorobyev†, N. Voytishin, B. S. Yuldashev[102], A. Zarubin, I. Zhizhin, A. Zhokin

† **Deceased**

1: Also at Yerevan State University, Yerevan, Armenia
2: Also at TU Wien, Vienna, Austria
3: Also at Institute of Basic and Applied Sciences, Faculty of Engineering, Arab Academy for Science, Technology and Maritime Transport, Alexandria, Egypt
4: Also at Ghent University, Ghent, Belgium
5: Also at Universidade Estadual de Campinas, Campinas, Brazil
6: Also at Federal University of Rio Grande do Sul, Porto Alegre, Brazil
7: Also at UFMS, Nova Andradina, Brazil
8: Also at Nanjing Normal University, Nanjing, China
9: Now at The University of Iowa, Iowa City, IA, USA
10: Also at University of Chinese Academy of Sciences, Beijing, China
11: Also at China Center of Advanced Science and Technology, Beijing, China
12: Also at University of Chinese Academy of Sciences, Beijing, China
13: Also at China Spallation Neutron Source, Guangdong, China
14: Now at Henan Normal University, Xinxiang, China
15: Also at Université Libre de Bruxelles, Brussels, Belgium
16: Also at University of Latvia (LU), Riga, Latvia
17: Also at An Institute or an International Laboratory Covered by a Cooperation Agreement with CERN, Geneva, Switzerland
18: Also at Helwan University, Cairo, Egypt
19: Now at Zewail City of Science and Technology, Zewail, Egypt
20: Also at British University in Egypt, Cairo, Egypt
21: Now at Ain Shams University, Cairo, Egypt
22: Also at Purdue University, West Lafayette, IN, USA
23: Also at Université de Haute Alsace, Mulhouse, France
24: Also at Department of Physics, Tsinghua University, Beijing, China
25: Also at Tbilisi State University, Tbilisi, Georgia
26: Also at The University of the State of Amazonas, Manaus, Brazil
27: Also at Erzincan Binali Yildirim University, Erzincan, Turkey

28: Also at University of Hamburg, Hamburg, Germany
29: Also at RWTH Aachen University, III. Physikalisches Institut A, Aachen, Germany
30: Also at Isfahan University of Technology, Isfahan, Iran
31: Also at Bergische University Wuppertal (BUW), Wuppertal, Germany
32: Also at Brandenburg University of Technology, Cottbus, Germany
33: Also at Forschungszentrum Jülich, Juelich, Germany
34: Also at CERN, European Organization for Nuclear Research, Geneva, Switzerland
35: Now at An Institute or an International Laboratory Covered by a Cooperation Agreement with CERN, Geneva, Switzerland
36: Also at Institute of Physics, University of Debrecen, Debrecen, Hungary
37: Also at Institute of Nuclear Research ATOMKI, Debrecen, Hungary
38: Now at Universitatea Babes-Bolyai-Facultatea de Fizica, Cluj-Napoca, Romania
39: Also at Physics Department, Faculty of Science, Assiut University, Assiut, Egypt
40: Also at HUN-REN Wigner Research Centre for Physics, Budapest, Hungary
41: Also at Punjab Agricultural University, Ludhiana, India
42: Also at University of Visva-Bharati, Santiniketan, India
43: Also at Indian Institute of Science (IISc), Bangalore, India
44: Also at Birla Institute of Technology, Mesra, Mesra, India
45: Also at IIT Bhubaneswar, Bhubaneswar, India
46: Also at Institute of Physics, Bhubaneswar, India
47: Also at University of Hyderabad, Hyderabad, India
48: Also at Deutsches Elektronen-Synchrotron, Hamburg, Germany
49: Also at Department of Physics, Isfahan University of Technology, Isfahan, Iran
50: Also at Sharif University of Technology, Tehran, Iran
51: Also at Department of Physics, University of Science and Technology of Mazandaran, Behshahr, Iran
52: Also at Italian National Agency for New Technologies, Energy and Sustainable Economic Development, Bologna, Italy
53: Also at Centro Siciliano di Fisica Nucleare e di Struttura Della Materia, Catania, Italy
54: Also at Università degli Studi Guglielmo Marconi, Rome, Italy
55: Also at Scuola Superiore Meridionale, Università di Napoli 'Federico II', Naples, Italy
56: Also at Fermi National Accelerator Laboratory, Batavia, IL, USA
57: Also at Consiglio Nazionale delle Ricerche-Istituto Officina dei Materiali, Perugia, Italy
58: Also at Riga Technical University, Riga, Latvia
59: Also at Department of Applied Physics, Faculty of Science and Technology, Universiti Kebangsaan Malaysia, Bangi, Malaysia
60: Also at Consejo Nacional de Ciencia y Tecnología, Mexico City, Mexico
61: Also at Trincomalee Campus, Eastern University, Sri Lanka, Nilaveli, Sri Lanka
62: Also at Saegis Campus, Nugegoda, Sri Lanka
63: Also at National and Kapodistrian University of Athens, Athens, Greece
64: Also at Ecole Polytechnique Fédérale Lausanne, Lausanne, Switzerland
65: Also at Universität Zürich, Zurich, Switzerland
66: Also at Stefan Meyer Institute for Subatomic Physics, Vienna, Austria
67: Also at Laboratoire d'Annecy-le-Vieux de Physique des Particules, IN2P3-CNRS, Annecy-le-Vieux, France
68: Also at Near East University, Research Center of Experimental Health Science, Mersin, Turkey
69: Also at Konya Technical University, Konya, Turkey
70: Also at Izmir Bakircay University, Izmir, Turkey
71: Also at Adiyaman University, Adiyaman, Turkey
72: Also at Bozok Universitetesi Rektörlügü, Yozgat, Turkey
73: Also at Marmara University, Istanbul, Turkey
74: Also at Milli Savunma University, Istanbul, Turkey
75: Also at Kafkas University, Kars, Turkey
76: Now at Istanbul Okan University, Istanbul, Turkey
77: Also at Hacettepe University, Ankara, Turkey
78: Also at Faculty of Engineering, Istanbul University-Cerrahpasa, Istanbul, Turkey

79: Also at Yildiz Technical University, Istanbul, Turkey
80: Also at Vrije Universiteit Brussel, Brussels, Belgium
81: Also at School of Physics and Astronomy, University of Southampton, Southampton, UK
82: Also at University of Bristol, Bristol, UK
83: Also at IPPP Durham University, Durham, UK
84: Also at Faculty of Science, Monash University, Clayton, Australia
85: Also at Università di Torino, Turin, Italy
86: Also at Bethel University, St. Paul, MN, USA
87: Also at Karamanoğlu Mehmetbey University, Karaman, Turkey
88: Also at California Institute of Technology, Pasadena, CA, USA
89: Also at United States Naval Academy, Annapolis, MD, USA
90: Also at Bingol University, Bingol, Turkey
91: Also at Georgian Technical University, Tbilisi, Georgia
92: Also at Sinop University, Sinop, Turkey
93: Also at Erciyes University, Kayseri, Turkey
94: Also at Horia Hulubei National Institute of Physics and Nuclear Engineering (IFIN-HH), Bucharest, Romania
95: Also at Texas A&M University at Qatar, Doha, Qatar
96: Also at Kyungpook National University, Daegu, Korea
97: Also at Another Institute or International Laboratory Covered by a Cooperation Agreement with CERN, Geneva, Switzerland
98: Also at Universiteit Antwerpen, Antwerpen, Belgium
99: Also at Yerevan Physics Institute, Yerevan, Armenia
100: Also at Northeastern University, Boston, MA, USA
101: Also at Imperial College, London, UK
102: Also at Institute of Nuclear Physics of the Uzbekistan Academy of Sciences, Tashkent, Uzbekistan